CHALMERS

Medfield DIAGNOSTICS

Development of UWB Antenna (0.5 - 5 GHz)
for Stroke Diagnosis

SHIRIN ABTAHI

Supervisor: Associate Professor Jian Yang

Department of Signal and System
Biomedical Engineering & Antenna Groups
CHALMERS UNIVERSITY OF TECHNOLOGY
Gothenburg, Sweden 2011
Master's Thesis 2011:EX075

Development of UWB Antenna (0.5 - 5 GHz) for Stroke Diagnosis

Abstract

Abstract

Keywords: Stroke Diagnosis, Microwave Tomography, UWB Antenna, Self-grounded Bow-Tie Antenna

The brain stroke is the third cause of death, ranking only behind heart disease and cancers. It also causes serious long-term disabilities which lead significant economic impact. Therefore, The real-time diagnosis is important because of different treatment; the ischemic stroke patients are given thrombolytic treatment which could be fatal for hemorrhagic patients. Currently, two stroke diagnosis techniques are in development, statistical classification and image reconstruction of human brain. The microwave based techniques need antennas which work in single or multi-frequency ranges. The multi-band operating systems are preferred due to higher resolution and deeper penetration than narrow band counterparts.

This project presents a compact ultra-wide multi-band (UWMB) antenna for stroke diagnosis over $0.5 - 5$ GHz — the miniaturized self-grounded Bow-Tie antenna immersed in a compact water cylinder. The self-grounded Bow-Tie antenna is a compact directional ultra-wideband antenna. By immersing the antenna in a compact distilled water cylinder, the impedance matching between the antenna and the human head is improved, the radiation leakage-out is reduced, and the size of the antenna is miniaturized significantly. These three characteristics are critical to antennas used in stroke diagnosis systems. An optimal design procedure is introduced due to the large simulation time. A prototype of the antenna has been manufactured. Simulated and measured data are presented for verification of the design, and some characteristics for the stroke diagnosis application are also discussed.

It should be noted that even this antenna development is focused on the stroke diagnosis application, the results can be easily extended or modified for other microwave medical applications, such as diagnosis of breast cancer or other cancers, cardiac imaging and medical monitoring.

Preface

This 30 credits thesis is for the degree of Master of Biomedical Engineering at Chalmers University of Technology. The work has been done at the Antenna Group, Department of Signals and Systems during February 2011 to September 2011.

Acknowledgements

Contents

List of Figures

List of Tables

1

Introduction

The brain stroke is the third cause of death, ranking only behind heart disease and cancers. It also causes serious long-term disabilities which lead significant economic impact. The current stroke diagnosis methods include Computed Tomography (CT), Positron Emission Tomography (PET) and Magnetic Resonance Imaging (MRI). The new non-invasive, mobile, real-time and easy to apply technique is Microwave Tomography (MWT). It is under development for diagnosis of breast cancer, lung cancer, brain imaging and cardiac imaging.

Medfield Diagnostics AB is an incubator company at Sahlgrenska hospital in Gothenburg. This company develops microwave based system which consists of helmet with ten microwave patch antennas and network analyzer as medical device for stroke diagnosis. The reflection and transmission data of all antennas are then processed to diagnose the stroke types, hemorrhagic and ischemic stroke. The final goal is providing a compact product for ambulances, so the proper stroke diagnosis can be made in earliest stage.

The existing stroke diagnosis system is presented in figure 1.1.

Figure 1.1: Existing stroke diagnosis system developed by Medfield Diagnostics (Stroke Finder)

The real-time diagnosis is important because of different treatment; the ischemic stroke patients are given thrombolytic treatment which could be fatal for hemorrhagic patients. Currently, two stroke diagnosis techniques are in development, statistical classification and image reconstruction of human brain. The microwave based techniques need antennas which work in single or multi-frequency ranges. The multi-band operating systems are preferred due to

higher resolution and deeper penetration than narrow band counterparts. This project focuses on design of UltraWide-Band antenna (UWB) which is ideal for multi-frequency techniques. [1]

1.1 Objective

The aim of this project is designing the compact immersed in water UWB antenna in frequency range of 0.5 to 5 GHz for brain stroke diagnosis system. The desired antenna should be small and directional with significant reduction in radiation leakage-out ratio.

1.2 Outline

An overview of the basic principles of brain stroke, MWT and antenna characteristic for medical application in chapter 2 will provide the background knowledge about project. The new design of antenna in chapter 3 includes simulation and parameter study of new design. Chapter 4 is concerned with the simulation and measurements results and discussions. Chapter 5 is mentioned the final conclusions. Finally, in chapter 6 the possible future work is described. The thesis's results are submitted to the IEEE Microwave and Wireless Components Letters, September 2011. [2]

2

Background

2.1 Brain Stroke

The brain is a most important part of Central Nervous System (CNS) which locates inside the skull. Under normal condition, brain uses glucose to supply its energy requirements. The brain's glycogen stores are negligible and depends on the continuous blood supply of oxygen and glucose. In fact, the decreasing of blood supply results most common problem of damage in the brain region. When lack of nutrition and oxygen occurred and neurons in the region confront lack of blood supply for even a few minutes, they stop functioning and die. This neuronal death results from vascular disease calls stroke.[3]

Since stroke treatment is depends on the type, the source of stroke and the location of injury,
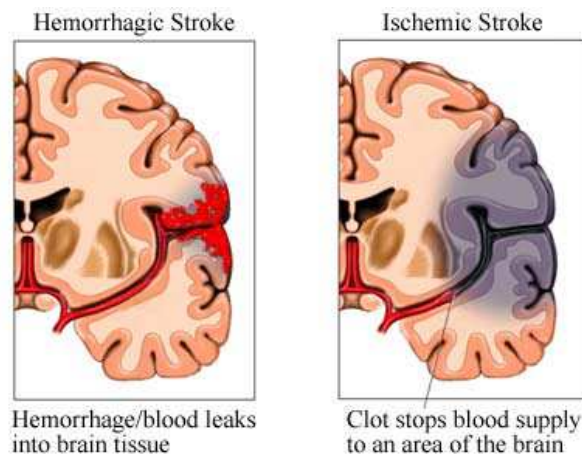
Figure 2.1: Ischemic and hemorrhagic stroke (Illustration copyright 2000 by Nucleus Communications, Inc)

stroke diagnosis in progress is critical. The stroke and Transient Ischemic Attack (TIA) have similar symptoms with other general medical conditions such as seizures, fainting, migraine and heart problems. Therefore, it is important to not diagnose as stroke. The stroke treatments are different according to type and play important role in medical diagnosis. Ischemic stroke, caused by blocked artery in brain and it may be treated with a clot-busting drug called tPA (tissue Plasminogen activator). If medical doctor diagnose ischemic stroke, it is important to receive drug treatment tPA within 4.5 hours of the onset symptoms. tPA cannot be given if

more than three hours passes. The hemorrhagic stroke is result of a ruptured blood vessel or a week area of blood vessel that bulges.[4] The difference between ischemic and hemorrhogic stroke is depicted in figure 2.1.

There are several diagnostic exams that can perform to know if someone has a stroke or is at risk of having it:

- Computed Tomography (CT) is the first test which generate detailed picture of brain to conform the stroke diagnosis and tell whether the stroke is hemorrhage or ischemic.

- Magnetic Resonance Imaging (MRI) performs to identify the site and source of the stroke. It may identify the place deprived of sufficient blood flow.

- Angiography is an X-ray to highlight the blood vessels by injecting the contrast agent into a vein. In this exam the radiologist can understand the exact place of blocking or bleeding in the brain. It also uses to lead catheters to the site of problem and do treatments. [4]

- Microwave Tomography which will explain more in 2.2 is under development exam that can be done in early stage of stroke even in ambulance to further treatment.The longer the brain cells are deprived of oxygen, the more damage they will suffer. Therefore, an early treatment after a stroke is extremely important.

2.2 Microwave Tomography Overview

Electromagnetic radiation classifies according to increasing of frequency and consists of radio waves, microwave radiation, visible light, ultraviolet radiation, X-rays and gamma rays. Microwave Tomography (MWT) is defined as using of electromagnetic wave-field imaging in the microwave frequency range from a few hundred MHz to approximately 10 GHz. Table 2.1 indicate approximate frequency and wavelength for common region of electromagnetic radiation. The biological tissues have different properties in microwave spectrum and therefore,

Table 2.1: Spectrum of electromagnetic radiation

Class	Frequency(Hz)	Wavelength (m)
Radiowaves	$< 3 \cdot 10^8$	$> 10^0$
Microwaves	$3 \cdot 10^8 - 3 \cdot 10^{11}$	$10^{-3} - 10^0$
Infrared	$3 \cdot 10^{11} - 4 \cdot 10^{14}$	$7.5^{-7} - 10^{-3}$
Visible light	$4 \cdot 10^{14} - 7.5 \cdot 10^{14}$	$4^{-7} - 7.5^{-7}$
Ultraviolet	$7.5 \cdot 10^{14} - 3 \cdot 10^{17}$	$10^{-9} - 4^{-7}$
X-rays	$3 \cdot 10^{17} - 3 \cdot 10^{19}$	$10^{-11} - 10^{-9}$
Gamma-rays	$> 3 \cdot 10^{19}$	$< 10^{-11}$

they can be imaged based on their dielectric properties. It is known that dielectric properties is related to water content of tissues for instance muscle have low while fat and bone have high water content.[1] There is a large difference between X-rays and microwave wavelength as table 2.1. Therefore, they behave differently when encounter dielectic objects such as human body. X-rays penetrate straight, while microwaves scatter on the molecules of human tissue.

The clinical decision for diagnosis relies on imaging methods such as CT, PET and MRI which each gives useful information according to the tissue properties. Each of these methods has their advantages but none of them is a cost effective solution in the emergency department.

Since MWT is a safe, portable and cost-effective solution, it could be a good supplement for current imaging methods.[5] MWT is based on microwave scattering measurements from the target. Then the image will be reconstructed from these measurements. The image reconstruction in MWT is in general a very complex and time consuming.

The general setup for MWT consists of array of antennas, switching matrix, network analyzer and computer for image reconstruction. The network analyzer is a general instrument for transmitting and receiving electromagnetic waves. The switching matrix is used to couple in and out antennas pairs for transmitting and receiving to measure every antenna combination in the setup. In general, the more sources/receiver will lead better quality of reconstructed image. However, an increase of the antenna numbers will cause problem such as increase of data acquisition time and problem related to design and construct small efficient antennas. The actual image generates by reconstruction software. The reconstruction software is using analytical or semi-analytical algorithm utilizing linear approximations such as Born and Rytov approximations. The new method is iterative nonlinear reconstruction algorithm were developed by a Chew and Wang. The iterative nonlinear methods is using a cost function which should be minimize or maximize. To achieve the best resolution, high frequency components should use as much as possible. In the other hand, it could lead algorithm easily get trapped in local minima. To overcome this problem, a priori information about the object or multi-frequency algorithms can be used. The frequency-hopping approach is a multi-frequency algorithm which stabilizing the reconstruction by using low frequencies while providing improve resolution by using high frequencies.[6]

2.3 Antenna Characterization

This part tries to give an overview about antenna characterizations which will need for following the report. The audience with background of antenna engineering could skip this part.

2.3.1 Radiation Pattern

The radiation pattern is an important concept which can easily indicate the application of antenna. For instance, cell phones needs nearly omnidirectional antenna because of the unknown user's location. In the other hand, for satellite applications a high directive antenna is desired.[7]

According to antenna theory an antenna radiation pattern is defined as follows: "An antenna radiation pattern is a mathematical function or graphical representation of the radiation properties of an antenna as a function of space coordinates. The radiation properties include radiation intensity, field strength, directivity, power flux density, phase or polarization." the two or three dimensional spatial distribution of radiated energy as a function of observer's position along a path is one of the most desired radiation properties.[8] The Bow-Tie antenna and its radiation pattern depict in figure 2.2.

2.3.2 Radiation Intensity

Radiation intensity is defined as "the power radiated from an antenna per unit solid angle". It is a far-field parameter and it can be achieved by multiplying the radiation density by the square of the distance.[8]

$$U = r^2 W_{rad} \qquad (2.1)$$
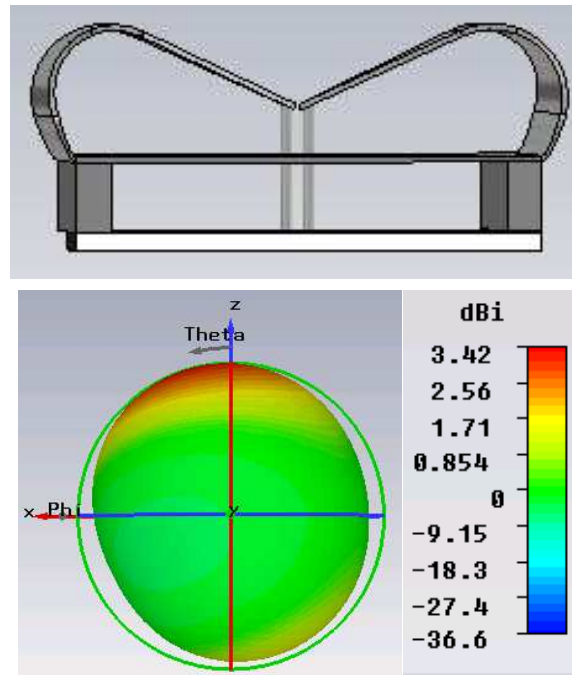
Figure 2.2: The radiation pattern of the Bow-Tie antenna; The radiation pattern shows the most radiation towards the Bow-Tie head in Z direction

2.3.3 Directivity

The antenna directivity is defined as "the ratio of the radiation intensity in a given direction from the antenna to the radiation intensity averaged over all directions".[8] It can be written as

$$D = \frac{4\pi U}{P_{rad}} \tag{2.2}$$

where
D = directivity
U = radiation intensity ($W/unit\ solid\ angle$)
P_{rad} = total radiated power (W)

2.3.4 Antenna Efficiency

Losses at the input antenna terminals and within the antenna structure is the total antenna efficiency e_0. such losses are due to reflection because of mismatch between the antenna and the transmission line and I^2R losses from conduction and dielectric.[8]

The overall efficiency can be written as

$$e_0 = e_r e_c e_d \tag{2.3}$$

where
e_0 = total efficiency
e_r = reflection (mismatch) efficiency = $(1 - |\Gamma|^2)$
e_c = conduction efficiency
e_d = dielectric efficiency
e_0 = total efficiency
Γ = voltage reflection coefficient at the input terminals of the antenna

$$\Gamma = \frac{(Z_{in} - Z_0)}{(Z_{in} + Z_0)} \tag{2.4}$$

where
Z_{in} = antenna input impedance
Z_0 = characteristic impedance of the transmission line

The scatter parameter or S-parameter describe the input-output relationship between terminals. For instance, S12 represent the power transfered from port1 to port2. The voltage reflection coefficient at the terminals of antenna (Γ) shows how much power is reflected form the antenna and also is called S11. If S11 = 0 dB, all the power is reflected from the antenna and nothing is radiated. This also means that the voltage reflection coefficient (Γ) equals to one. The typical reflection coefficient S11 for antenna is depicted in figure 2.3. It is obvious that the
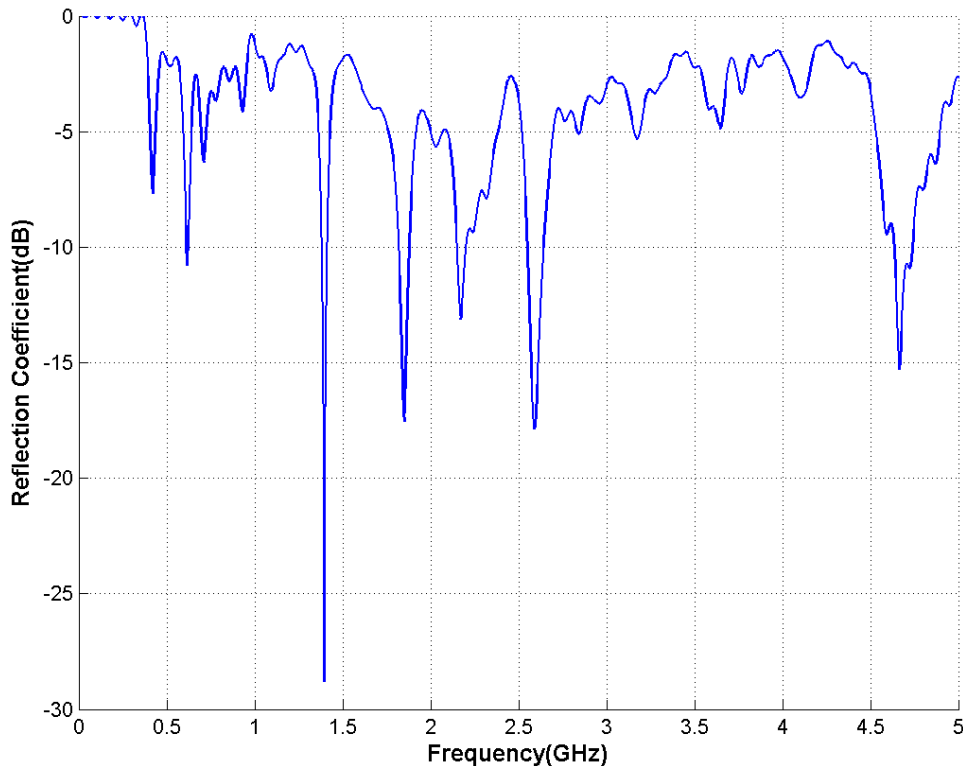
Figure 2.3: The voltage reflection coefficient at the input terminal of antenna (S11) in dB

antenna radiates best at 1.4 GHz, where S11 = -28 dB. This means that the antenna reflection for this frequency is negligible.

In this work, antenna operates in near-field environment.The antenna functions partly as an impedance transformer from 50 Ω coaxial connector to the impedance of area of detection in

human head. The reflection coefficient Γ at the input coaxial port indicates how much the signal is transmitted into the area of detection. Therefore, it should be the performance including the human head.

2.3.5 Radiation Leakage-out Ratio

In stroke diagnosis, it is preferred that all detection signal is transmitted to the area of detection in human head. In practice, there is always radiation leakage-out into free space. The radiation leakage-out ratio L_{rad} measures the part of signal not into the area of detection and it is the ratio of the power radiated out into free space P_{rad} to the transmitted power P_{trans}, see figure 2.4.

$$L_{rad} = \frac{P_{rad}}{P_{trans}} \tag{2.5}$$
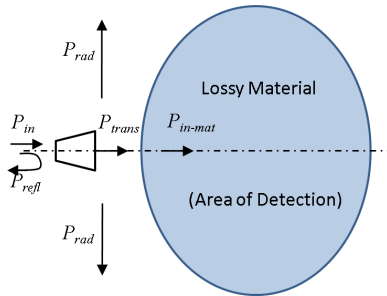
Figure 2.4: Radiation Leakage-out

In an array antenna, the radiation leakage-out will cause interference among the antenna elements via mutual coupling in free space without any information of the area of detection. Therefore, the lower radiation leakage-out ratio will cause the better performance of the antenna for such applications.

The radiation leakage-out ratio is the same as the radiation efficiency defined in [9], but using the present terminology emphasize on different performance for different applications.

2.3.6 Bandwidth

The bandwidth of an antenna is defined as the range of frequencies which the antenna is performed due to some characteristic and it can be considered as a range of frequencies on either side of the center frequency. The bandwidth in broadband antennas is expressed as the ratio of upper to lower frequencies of acceptable region and in narrow-band antennas, it is expressed as a percentage of the upper frequency minus lower frequency over the center frequency of the bandwidth.[8]

Ultra Wide-Band (UWB) have very large bandwidth, typically more than 500MHz. The UWB antennas are widely in attention in communication systems because of very high bandwidth and low power requirement. The aim of this project is to design a UWB antenna which works in the 0.5 - 5 GHz frequency range.

2.4 The Medfield existing Antenna in stroke diagnosis system

The current narrow-band antenna in Medfield Company is using microstrip technology with triangular shape as it depicts in figure 2.5. The main features of this system are small size,
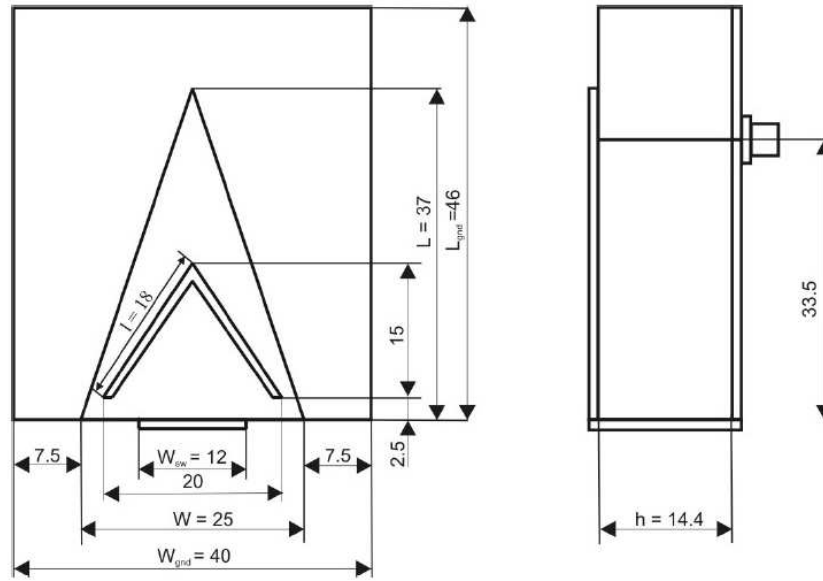
Figure 2.5: Triangular patch antenna uses in existing Medfield system

low cost and light weight but the bandwidth is limited. To enhance the limited bandwidth, the design includes cutting of various shape of slot in patch. Therefore, current along the slot edges cause additional resonance, in combination with the main patch resonance.

The geometry of antenna is as below:

- The triangular patch antenna with the length of $L = 37mm$ and $W = 25mm$. It is printed on the dielectric substrate with permittivity of $e_r = 2.34$ and thickness of $h = 14.4mm$.

- The substrate and ground plane have rectangular shape of length $L_{gnd} = 46mm$ and $W_{gnd} = 40mm$.

- The V-shaped slot with $1mm$ width is centered in the triangular patch and tip is facing with triangle tip. The outer edge is $l = 18mm$ with distance of $d = 2.5mm$ from the patch bottom side. The shorting wall dimension is $W_{sw} = 12mm$.

- The antenna is excited by a prob-feed via the coaxial transmission line places at the center of the patch at the distance of $d_f = 3.5mm$.

If the antenna moves closer or further from the head, the impedance matching quality degrades. Since the same distance of all antennas from the head cannot be guaranteed, placing the matching liquid is appropriate. The water bag as a lossy medium with relative permittivity 78 places between the antenna and the head to affects the impedance matching. This improves and unifies the impedance matching between antennas and head.[10]

2.5 Overview of UWB Antenna Research activities at Antenna Group at Chalmers

Ultra Wide Band (UWB) systems use electromagnetic signals with greater than 500MHz bandwidth or 20% bandwidth around the center frequency. UWB systems have some advantages including of high data rate, low transmit power, low interference and availability of low cost

transceiver. Therefore, they can be used for portable commercial applications. In UWB systems because of wide bandwidth, the antenna parameters are frequency dependent. Therefore, the analysis and design are complicated. Many UWB antennas have been developed, for example, Bow-Tie dipoles [11],biconical dipoles [12], log-periodic dipole arrays [13]-[15], self complementary spiral antennas [16], Vivaldi antennas [17], and recently developed self-grounded Bow-Tie antenna [18].

The Vivaldi antenna is one of the UWB antennas which was first investigated in 1979 [19] and then some improvements have been done based on initial design. It is a planar traveling wave antenna with end-fire radiation. Since Viavaldi antennas have wide bandwidth, low cross polarization and highly directive pattern, it is one of the most used antennas for UWB applications[20]. The model 3164-08 Open Boundary Quad-Ridged Horn antenna is another example of UWB antenna from ETS-Lindgren. Since it has highest gain in the 5.8 GHz range, this antenna is ideal for WiMAX. Additional applications include UWB wireless testing (3 GHz - 10 GHz) and lower frequency testing (700 MHz - 3 GHz) for GSM, PCS, Wi-Fi etc. The frequency range is 700 MHz to 10 GHz and its compact design makes it ideal for use as a wall mounted or tripod mounted antenna. It has low VSWR with improved gain.

During recent years the Antenna Group at Chalmers has developed several new UWB antennas for different applications and drawn a lot of attention in the international antenna&propagation society. Below are the examples.

The Eleven antenna is a compact, low-profile decade-bandwidth log-periodic dual-dipole array antenna [14][15], [21]-[26]. It has many advantages: a constant phase center location, constant beam width over a decade bandwidth, high BOR_1 efficiency, low cross polar level and good reflection coefficient, all over a decade bandwidth. Therefore, it is very suitable to be a feed for reflector antennas for future UWB radio telescopes, such as the Square Kilometer Array (SKA) [27] and the Very Large Baseline Interferometry 2010 (VLBI2010) [28].

Hat feed is a waveguide self-supported feed for reflector antennas [29]-[34]. It has many advantages: low cross polarization level due to the similar E- and H-plane radiation functions, low far-out sidelobes, low blockage as no struts needed to support the feed, and low ohmic loss since the electronic devices (such as transceiver) can be placed directly behind the reflector. During the recent years, the band width of the hat feed has been improved to be tripled of the previous one and therefore can be applied in satellite communication systems [35]-[36].

Self-grounded Bow-Tie antenna is a compact, low profile and directional UWB antenna [37][18], which is very suitable for UWB radar systems [38][39].

2.6   Electromagnetic Fields Safety

The International Commission on Non-ionizing Radiation Protection (ICNIRP) is guidelines to limit Electromagnetic Field (EMF) exposure that will provide protection against known adverse health effects. The ICNIRP guideline consists of basic restrictions and reference levels. The basic restrictions are restrictions on exposure to time varying electric, magnetic and electromagnetic fields. The physical quantities used to specify basic restrictions are current density (J), Specific energy Absorption Rate (SAR) and power density (S). The basic restrictions requires to not exceed for protection against adverse health effects. The reference levels of exposure are physical quantities which can compare with measured values. If measured values compliant with all reference levels, it will compliant with basic restrictions. On the other hand, if measured values are higher than reference levels, more detailed analysis is necessary. However, it does not essentially means that the basic restriction are exceeded. The exposure limitation is established for occupational and general public. The occupationally exposed population

are adults which exposed under known condition. They are trained to be aware of potential risks and to take suitable protections. The general public are individuals of all age with varying health status. Members of public are unaware of their exposure to EMF and cannot be expected to take proper protections.

According to ICNIRP guideline the basic restrictions for EMF for frequencies up to 10 GHz," between 100 KHz and 10 GHz basic restrictions on SAR are provided to prevent whole-body stress and excessive localized tissue heating". SAR is the rate of energy absorption by the body when exposed to EMF. It is defined as power absorbed per mass of tissue and measure with watts per kilogram (W/kg). SAR is usually averaged over the whole-body or a small sample volume for instance, 1 g or 10 g of tissue. The localized SAR limitations for head and trunk in ICNIRP are 10 W/kg and 2 W/kg for occupational and general public exposure respectively. All SAR values should be averaged over any 6 min period. values of SAR depends on the incident field parameters, the characteristics of exposed body and ground effects and reflector effects of other objects in the field near the exposed body.

For simultaneous exposure to multiple frequency fields, the exposures are additive in their effects. SAR and power density values should be added according to equation 2.6.[40]

$$\sum_{i=100KHz}^{10GHz} \frac{SAR_i}{SAR_L} + \sum_{i>10GHz}^{300GHz} \frac{S_i}{S_L} \leq 1 \tag{2.6}$$

Where

SAR_i = The SAR caused by exposure at frequency i
SAR_L = The SAR limit given by ICNIRP
S_L = The power density limit given by ICNIRP
S_i = The power density at frequency i

3

Design of New Antenna
Compact Self-Grounded Bow-Tie
Antenna

The objective of this project is designing compact immersed in water Self-grounded Bow-Tie antenna which is directional. The small UWB antennas have advantages like high penetration ability, compact geometrical configuration and low interference level. The most of small UWB antennas for instance, Bow-Tie dipole, are omni-directional in radiation characteristic which is not desired here. Therefore, the self-grounded Bow-Tie which is invented by Professor Jian Yang uses as antenna model for this project. It is a tilted infinite Bow-Tie dipole which is located above the ground plane from geometric configuration view. Therefore, the antenna is frequency independent with directional radiation characteristics due to this configuration. The self-grounded Bow-Tie antenna is small with low profile in radiation direction. It has directional radiation characteristic and stable radiation beams for the frequency range of 2-15 GHz, ultra wide-band performance with about -10dB reflection coefficient and good time domain impulse response.[18]

The designed antenna is the modified version of self-grounded Bow-Tie antenna to make it smaller, mechanically more stable and suitable for whole system setup. The designed antenna from different point of view is depicted in figure 3.1.

3.1   Antenna Components

The designed antenna has several components which are summarized in table 3.1 and describe in more detail in this section.

1. The FR-4 Board is the woven glass fabric with epoxy resin binder which is flame resistant. It is almost used in the Printed Circuit Board (PCB) industry. In designed antenna it is used as substrate because it is cheaper and the order time is shorter compare to the other dielectric materials such as Rogress,TMM3 and TMM10. The FR-4 permittivity is 4.3 farads per meter (F/m). The FR-4 has different thickness which 1.6mm is selected to have more mechanical resistance. The FR-4 substrate is depicted in 3.2.

2. The Feeder Board is a Perfect Electric Conductor (PEC) plate which is placed on top of the grounded FR-4 substrate as in figure 3.3. The thickness of this board is 0.035mm.
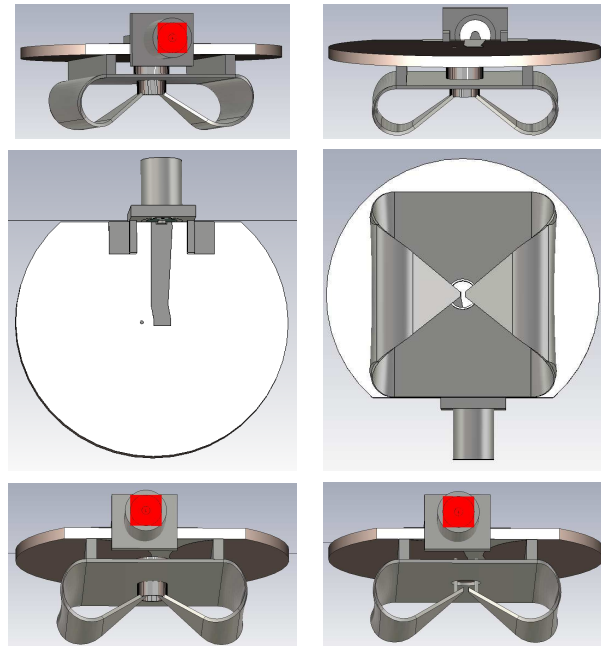
Figure 3.1: The designed antenna from different point of view
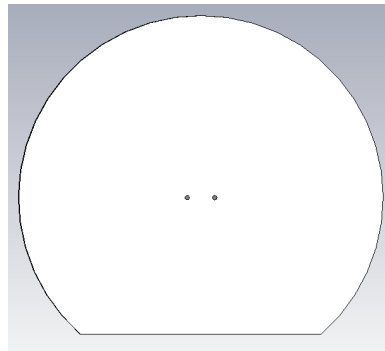
Figure 3.2: FR-4 Board used as substrate
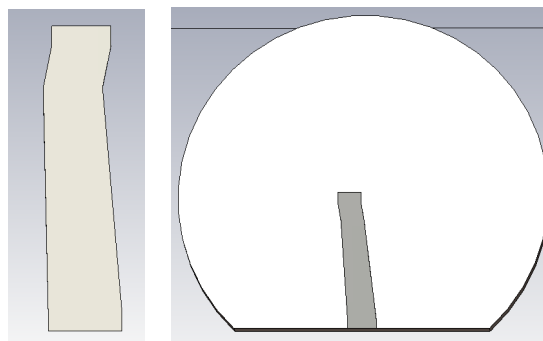
Figure 3.3: Feeder Board PEC plate on the grounded FR-4 substrate

3. The Ground Board is the other PEC plate which is placed on the other side of the FR-4 substrate board. The thickness of this metal sheet is also $0.035mm$. The ground plane is depicted in figure 3.4. These three parts of the design (Components 1 to 3) with feeder
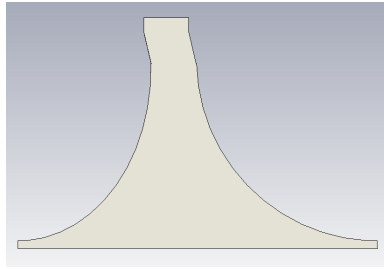
Figure 3.4: Ground Board placed at the other side of the FR-4 substrate

lines are called balun which is abbreviation of balance + unbalance. It is the type of electrical transformer which converts balanced impedance to unbalanced and vice versa.

4. The Feeder Lines or twin-wire transmission line are two Perfect Electric Conductor (PEC) lines which are connected to feeder board and the ground board to feed the antenna. Each of the feeder lines is cylindrical shape with 0.5mm diameter and center to center distance between these two feeder lines is 3mm. The feeder lines are connected to the head of self-grounded Bow-Tie head from the other side. The feeder lines are depicted in figure 3.5 from different point of view.
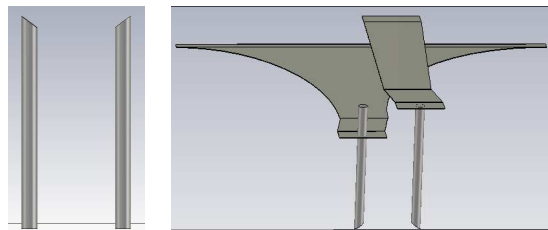
Figure 3.5: Feeder lines from different point of view

5. The Antenna Plate consists of three PEC plates which form the head of the Bow-Tie antenna. There is a 20mm to 30mm PEC rectangular sheet which is joined from each side to the triangular shaped PEC plates. This plate is bended to form the tilted Bow-Tie. The actual plate shape is depicted in the left side of the figure 3.6. It is decided to make it easier for manufacturing by using the straight line for triangular parts.
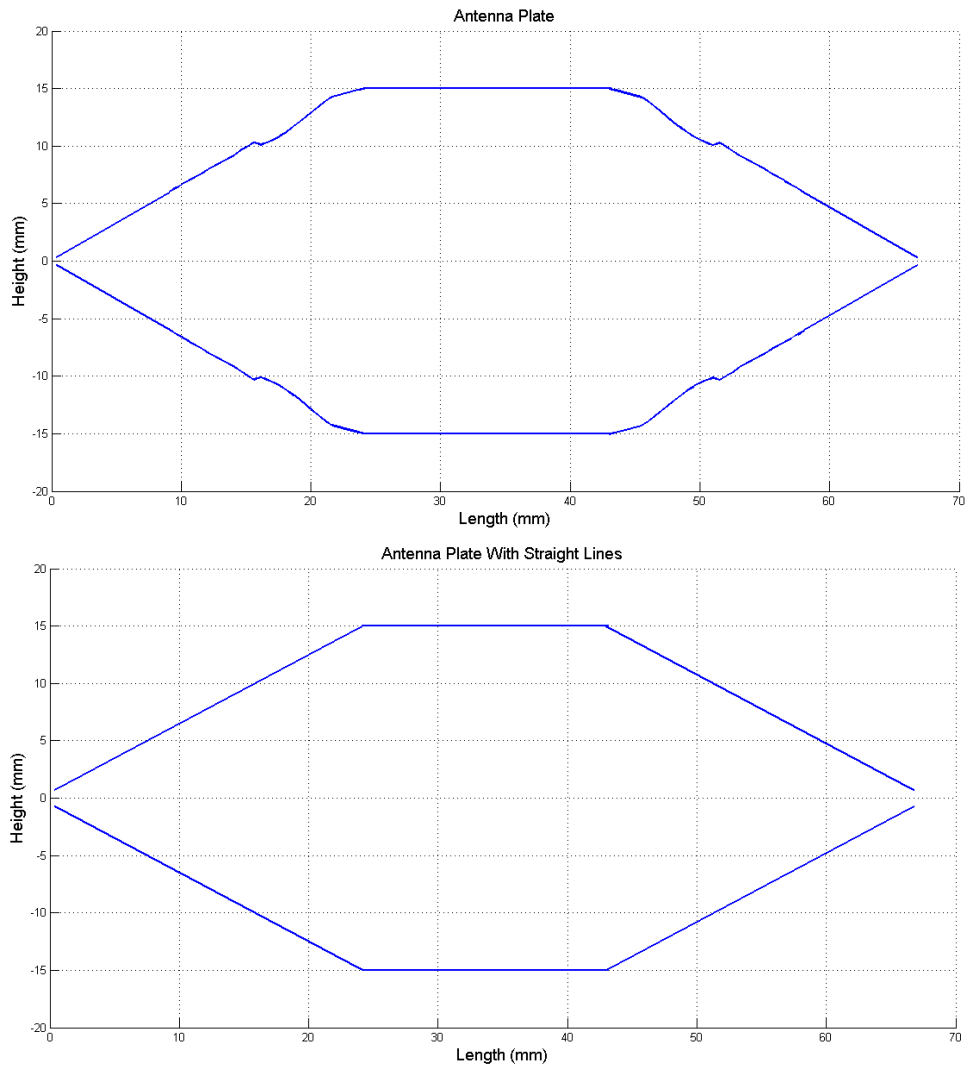
Figure 3.6: The Antenna Plate forms the tilted self-grounded Bow-Tie antenna head, to the top and the simpler plate uses for manufacturing to the bottom

6. The Teflon is fluorine plastic with physical properties which make it friction. The lossy Teflon is used as the support between the antenna plate and the head of the antenna for having more stability. The designed Teflon here consists of two hollow circular shaped mounted on top of each other and passes from the center of the antenna plate to the head of the Bow-Tie antenna while surrounds the transmission lines. This is depicted in figure 3.7.
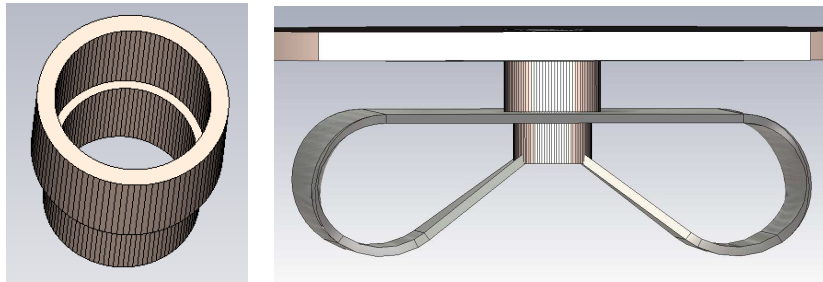
Figure 3.7: Teflon as support from FR-4 substrate toward the Bow-Tie antenna head and surrounds the feeder lines

7. The SMA (SubMiniature version A) Connectors are coaxial Radio Frequency (RF) connector. It is developed in the 1960s as a minimal connector interface for coaxial cable with a screw type coupling mechanism and has 50 ohms impedance. In this design the SMA right angle jack PCB with code 32K145-400L5 from Rosenberger Company is selected. The used SMA connector is depicted in figure 3.8.
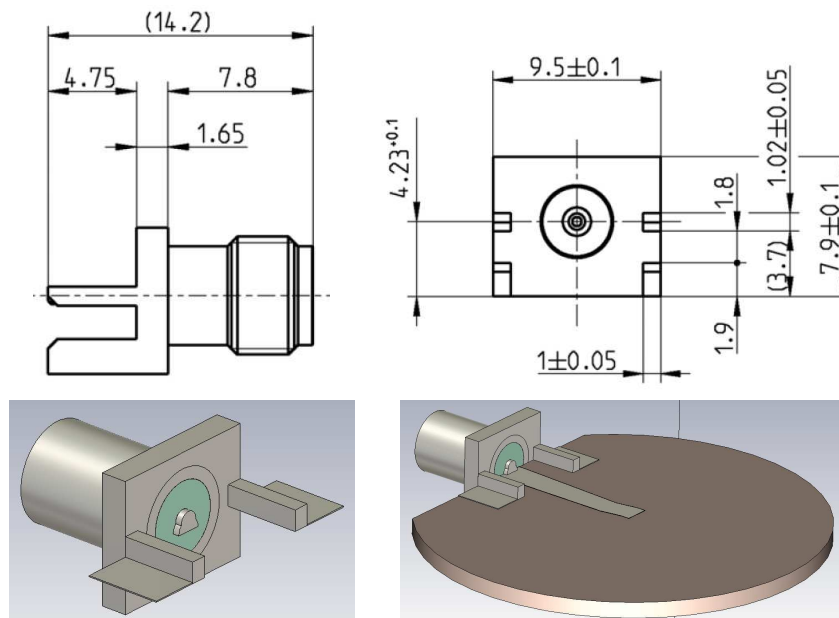
Figure 3.8: SMA right angle jack PCB with code 32K145-400L5 from Rosenberger company

Table 3.1: the antenna components with dimensions and connections

Components	Shape	Dimensions (*mm*)	Material	Connections
FR-4 Board		Radius = 20 Thickness = 1.6 a= 27.55 b = 3 c = 15	FR-4	Teflon Feeder lines Supports SMA connector
Feeder Board		a = 2.5 b = 1 c = 2.13 d = 1 W = 3.1 Thickness 0.035	PEC	Feeder lines
Ground Board		a = 2.5 b = 1 c = 2.13 d = 1 W = 3.1 Thickness 0.035	PEC	Feeder lines
Feederlines		a = 2.5 b = 1 c = 2.13 d = 1 W = 3.1 Thickness 0.035	PEC	Feeder Board Ground Board Bow-Tie antenna head
AntennaPlate		L1 = 20 a = 30 L2 = 15.15 b = 12 L3 = 9 c = 0.687	PEC	Supports
Supports		Height = 3 Length = 30 Width = 3	PEC	Antenna Plate FR-4 Board
Teflon		Top Teflon: Inner Radius = 2.2 Outer Radius = 2.7 Bottom Teflon: Inner Radius = 1.9 Outer Radius = 2.2	Teflon	FR-4 Board Antenna plate anotherTeflon Bow-Tie antenna head
SMAConnector		a: Radius = 0.6 b: Outer Radius = 2.28 Inner Radius = 0.6 c: Outer Radius = 3.02 Inner Radius = 2.28 Rect part: d = 9.5, e = 8 and f = 1.65 Two lags: Length = 4.8, Height = 1.3, thickness = 1 PEC sheet connect to lags: Length = 4.8, Height = 0.07, thickness = 3	PEC	Feeder Board
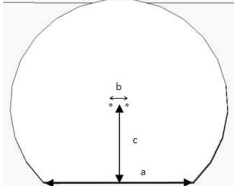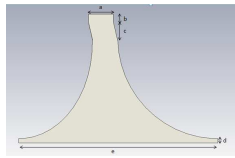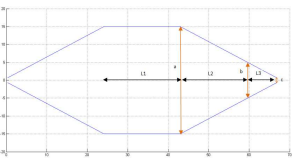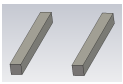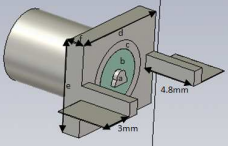
3.2   Antenna Design and Simulation

In this part the simulation tool, system setup and optimal design procedure are described.

3.2.1   Design and Simulation Tool

The design and simulation has done with a Computer Simulation Tool Microwave Studio (CST MWS). CST MWS 2011 is a specialist tool for the 3D electromagnetic simulation of high frequency components such as antennas, filters, couplers, planar and multi-layer structures. It enables accurate analysis of high frequency devices such as antennas. If study about the field propagating through a component is in attention, the real time domain simulation is particularly interesting. Besides the specific capabilities in time domain, the Transient Solver also delivers broadband frequency domain results like S-parameters. The field results for many frequencies can be derived from one single simulation run. The time domain and frequency domain solvers are available. However, only the time domain solver is used in this project. [41]

3.2.2   System Setup

The idea is using the antenna in simulated environment which has similar dielectric properties as human head.The dielectric properties of biological tissue as a function of frequency from 10 Hz to 100 GHz at 37°C are studied by Gabriel and reported in [42]. Also, there is another study on permittivity of the human gray matter from 18°C to 25°C and at 37°C in [43]. The dielectric properties of human brain gray matter from these studies are summarizes in table 3.2. According to this table, the permittivity of the skull is considered as 50 (F/m) in simulation.

Table 3.2: Comparison of dielectric properties of gray matter from different studies

Studies (mean ± SD)	900 MHz	1025 MHz	1080 MHz
human, measured @ 18°C to 25°C	57.8 ± 3.3	57.4 ± 3.3	57.1 ± 3.4
human, measured @ 37°C	55.5 ± 3.1	55.1 ± 3.2	54.9 ± 3.3
Gabriel et al., 1996b, human, measured @ 37°C	–	50.5 ± 2.5	–

The simple simulated environment consists of antenna, water bag and head phantom. In this work, the antenna is used as a kind of sensor in near field environment so the head should be involved in the antenna design. Since the computation with real phantom model in CST takes almost four days to have one simulation on a powerful PC with 16 cores and 72 GB memory, the simple phantom model is used during design procedure to make it feasible and more efficient. The real phantom model is used only for simulation of final design.

For the sake of patient comfort, a water bag or other soft bag should be used between the antenna and human head. Thus, a water bag is used as a part of new antenna, in other words, immerse the antenna in water. It has the following advantages:

1. It is used to improve impedance match between antenna and human head. The water bag is the cylindrical Polyoxymethylene (POM) fills with distilled water with 78.4 (F/m) permittivity while the permittivity of the human brain is approximately 74. Note that between distilled water and the brain exists the skull with permittivity of 50, which makes the UWB performance of reflection coefficient very difficult for the whole antenna system. Therefore, an ultra-wide multi-band (UWMB) performance is more realistic for the antenna in this work. The water bag diameter is 20*mm* and the Simple head Phantom

is a cylindrical shaped with $49mm$ diameter. The whole system setup and the antenna immersed in water is indicated in figure 3.9 and figure 3.10 respectively.
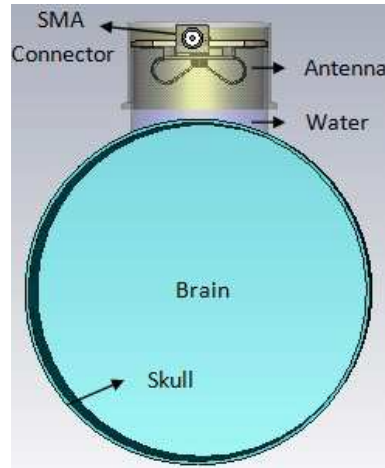
Figure 3.9: The whole system setup with simple phantom model
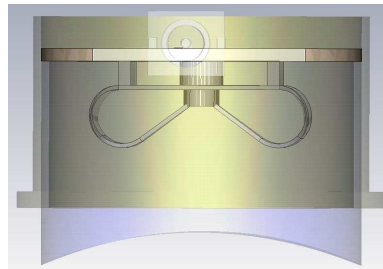
Figure 3.10: Antenna places in water with Polyoxymethylene wall

2. The radiation leakage-out can be reduced because the water cylinder functions as a guide for the wave propagation from the antenna to the head.

3. The size of the antenna can be miniaturized significantly due to the high permittivity of distilled water.

The simulation results are divided into two models, with shell and without shell as model the human skull. The permittivity of this shell (skull) according to table 3.2 is considered as 50 (F/m) and the Shell diameter is $50mm$. Therefore, there is 1 mm space between skull and the inside head liquids as in figure 3.9. The top FR-4 board is used for connecting the antenna to the helmet.

The average length of an adult skull from the forehead to occiput is around 21 to $22cm$ and the average width is about 17 to $18cm$. The circumference of an adult skull is averaged from 54 to $57cm$. The simulation phantom model have average mentioned dimensions and its shape consists of skull and face (mouth, nose, ear etc). The perfect system uses the CST phantom model as a model of human head. It uses in simulation of the final design due to complexity as mentioned before. The CST MWS phantom model depicts in figure 3.11.
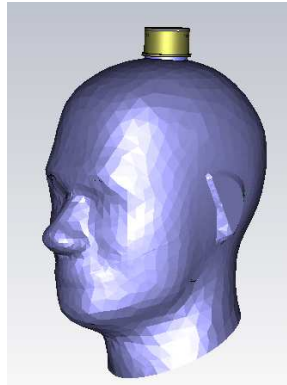
Figure 3.11: The CST MWS phantom model as human brain with one antenna

3.2.3 Optimal Design Procedure

The impedance matching between different parts of the antenna is the important issue in design. In order to match the impedance of feeder lines with metallic feeder board on the FR-4 board, the characteristic impedance of two conductor transmission lines with circular cross section can be calculated with equation 3.1 as in [24]. The cross section of the transmission lines depicts in figure 3.12.

$$Z_0 = \frac{1}{\pi}\sqrt{\frac{\mu_0}{\epsilon_0 \epsilon_r}} \cosh^{-1}\frac{D}{d} \tag{3.1}$$

where
$\mu_0 = 4\pi \times 10^{-7}$
$\epsilon_0 = 8.85 \times 10^{-12}$
$\epsilon_r = $ The material permittivity which two transmission lines place in
$D = $ Center to center feeder line (Transmission line) distance
$d = $ The transmission line diameter The unknown parameter in equation 3.1 is the center to
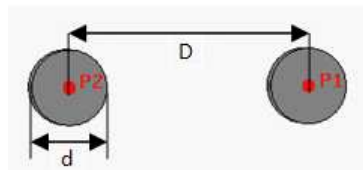
Figure 3.12: Two conductor transmission line with circular cross section

center feeder lines distance (D) by using the characteristic impedance Z_0 (50Ω). Since in this design the transmission lines are connected to the Bow-Tie antenna head, the equation 3.1 does not result the true impedance matching value. Therefore, the feeder lines distance are changed by trial and error and check the reflection coefficient results to understand which distance is more proper for impedance matching. In order to achieve true impedance matching, the design problem is solved with following procedure:

Design the antenna in the background of water

First the self-grounded Bow-Tie antenna in the background of distilled water for the frequency range of 0.5 to 5 GHz is designed as shown in figure 3.13. Therefore, the problem includes only

the antenna without the feeding structure and the head and it is much smaller than that with feeding and the head. Thus, the parameter study was carried out for an optimal design. The computation time is still very large about half day.
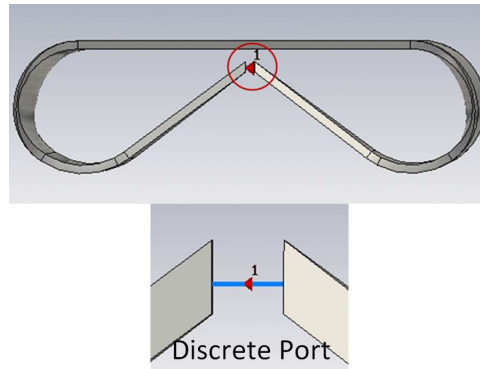
Figure 3.13: The antenna in the background of water

Design the twin-line feeding including the head model

In this stage, a simple model of human head, a cylinder with a thin layer as skull and the rest as brain, was included as shown in figure 3.14. The inner Teflon support, a hollow cylinder through the ground plane, is designed for mechanical stability, and the outer POM cylinder is as the water holder. The impedance is calculated by removing the feeder board and ground board, removing FR-4 Board and using multi pin waveguide for simulation. Due to the large simulation time in CST, a parameter study on the space D and the diameter of lines d is performed.
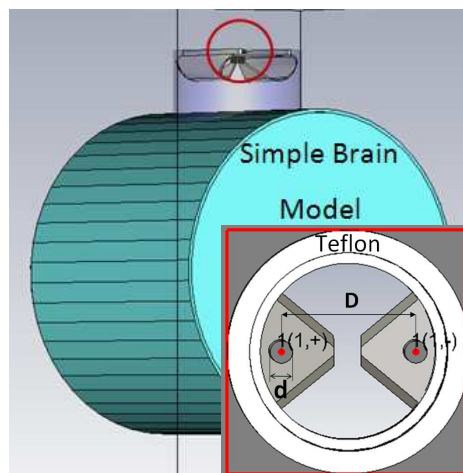
Figure 3.14: Calculating the impedance line of antenna by removing the FR-4 board, feeder board and ground board by using multipin waveguide for simulation

Design the compact balun

The third step was designing the compact balun – transformer from a microstrip line with a 50-Ohm characteristic impedance to the 42.6-Ohm twin-line feeding in water, see the model in

figure 3.15. This was a bit challenge for the design because the balun should be very compact. Waveguide ports were used in the CST model. The substrate material, the thickness of the board, the width of the line and the shape of the ground plane are the parameters tuned for the optimal performance.
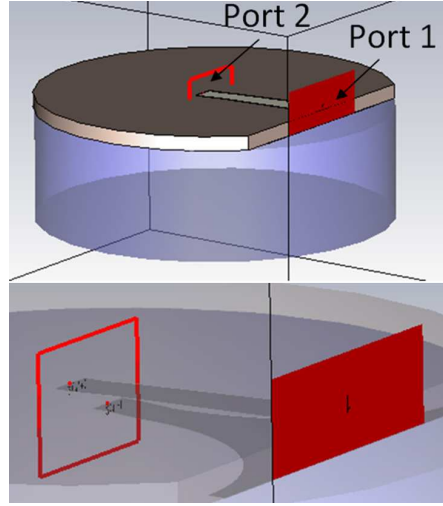
Figure 3.15: Calculating the impedance line of the microstrip transmission line by removing the antenna tilted head

The characteristic impedance of the microstrip transmission line is reported by Wheeler and Schneider. It is expressed for Z_0 and ϵ_{reff} as in equation 3.2 to 3.7 and parameters are shown in figure 3.16.[44]

$$Z_0 = \frac{60}{\sqrt{\epsilon_{reff}}} \ln(\frac{8}{W_e/h} + 0.25\frac{W_e}{h}), \qquad W/h \leqslant 1 \qquad (3.2)$$

$$Z_0 = \frac{120\pi}{\sqrt{\epsilon_{reff}}} \left[(\frac{W_e}{h} + 1.393 + 0.667\ln(\frac{W_e}{h} + 1.444) \right]^{-1}, \qquad W/h \geqslant 1 \qquad (3.3)$$

where

$$\frac{W_e}{h} = \frac{W}{h} + \frac{1.25}{\pi}\frac{t}{h}(1 + \ln\frac{4\pi W}{t}), \qquad W/h \leqslant \frac{1}{2\pi} \qquad (3.4)$$

$$\frac{W_e}{h} = \frac{W}{h} + \frac{1.25}{\pi}\frac{t}{h}(1 + \ln\frac{2h}{t}), \qquad W/h \geqslant \frac{1}{2\pi} \qquad (3.5)$$

$$\epsilon_{reff} = \frac{\epsilon_{r+1}}{2} + \frac{\epsilon_{r-1}}{2}\left[(1 + \frac{12}{W/h})^{-1/2} + 0.04(1 - \frac{W}{h})^2\right] - C, \qquad W/h \leqslant 1 \qquad (3.6)$$

$$\epsilon_{reff} = \frac{\epsilon_{r+1}}{2} + \frac{\epsilon_{r-1}}{2}(1 + \frac{12}{W/h})^{-1/2} - C, \qquad W/h \geqslant 1 \qquad (3.7)$$

where
h =Dielectric Thickness
t =Track Thickness
W =Track Width
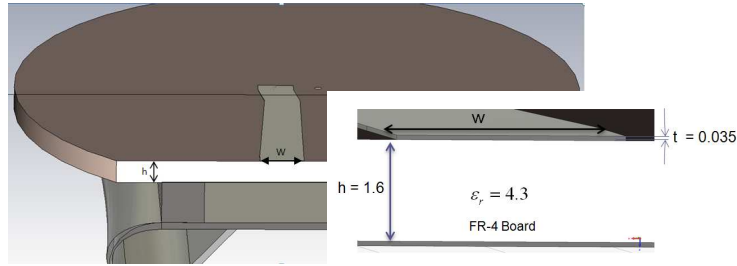
Figure 3.16: The parameters used to calculate width of the microstrip line

The aim is designing the model which have the same antenna impedance line as the transmission lines. Since the port-1 is connected to the 50Ω coaxial cable, the desired characteristic impedance Z_0 in the equations 3.2 to 3.7 is 50Ω. Therefore, W will calculate $3.1mm$ by using FR-4 board with 4.3 (F/m) permittivity. The characteristic impedance of port-2 should change to reach the desired value by changing the substrate material or changing the feeder board width from top as it is shown in section 4.

Combine all parts

The final step is to combine all parts together, as shown in figure 3.9. The results are shown in next section.

3.2.4   Two Antennas in front of each other

The two antennas in the water bag are placed toward each other to study how much power is radiated out (leakage) and study if antenna is directional. The position of antennas is depicted in figure 3.17. The following term 3.8 is used to measure how much power is absorbed the head.
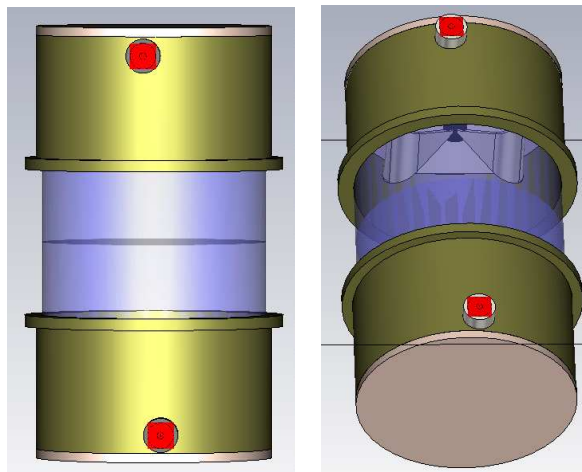
Figure 3.17: Two antennas in front of each other to study how much power is radiated out

$$L_r = 10log_{10}(|S11|^2 + |S12|^2) \tag{3.8}$$

3.3   Antenna Measurements

In this part, the equipment and tools for measurements and the system setup are explained.

3.3.1   Measurement's Equipments

The common environment for measurement of antenna characterization is Reverberation Chamber (RC). The RC is also called a mode stirred chamber, consists of sufficient large, rectangular metal cavity to support many resonant modes which are stirred by movable object inside the cavity. The movable stirred inside the chamber creates an independent field distributions. this independent field distributions represent a statistically isotropic field. This means that the test object will receive signals from all directions and it is a multi-path environment.

The radiation efficiency is one of the most important performance parameter of an antenna which can be measured in the reverberation chamber. The RC performs high accuracy even in the small dimensions. The measurements in reverberation chamber are fast, easy to make and repeatable even in equal or larger chambers. These advantages motivate using of reverberation chamber for antenna measurements. The figure 3.18 shows the BLUETEST reverberation chamber and Aglient E5071C network analyzer which is used in this project.

Figure 3.18: The BLUETEST reverberation chamber and the Aglient E5071C network analyzer; Chalmers antenna group

The phantom head used for measurement is plastic head model which is filled with 60% water, 36% sugar and 0.1% salt to model the healthy brain, shown in Fig.3.19.

Figure 3.19: The phantom head in measurement

24

3.3.2 Measurement's Setup

In ordet to measurement of radiation efficiency, first the reference antenna (disk-cone antenna) is mounted the PCV stand to do the reference measurement. The same load has to be present in the RC during the reference and efficiency measurements. Therefore, The AUT (Antenna Under Test, i.e., phantom head in measurement with one antenna) is terminated and placed in the chamber. When the reference measurement has been performed, terminate the reference antenna and put it on the floor of the chamber. Put the AUT on the platform and connect it to the port for efficiency measurement. The difference between power level in dB in these two step gives the radiation efficiency. The efficiency measurement shown in figure 3.20.

Figure 3.20: Efficiency measurement in reverberation chamber

4

Results and Discussion

4.1 Simulation Results

In this section the simulation results of optimal design procedure and final design are discussed.

4.1.1 Simulation results of antenna in the background of water

The antenna reflection coefficient in the background of water is depicted in figure 4.1. This shows that most of the power is radiated and the reflected power is small.
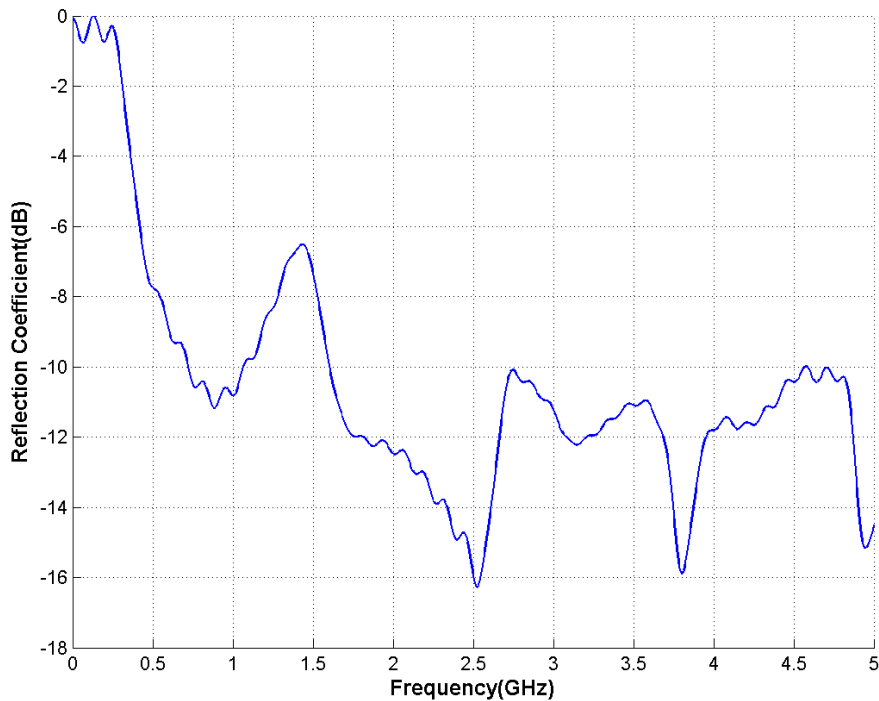

Figure 4.1: The antenna S-parameter results

4.1.2   Optimal design procedure

The feeder lines center to center distance changes by trial and error in design of the twin-line feeding including the head model (section 3.2.3) and the reflection coefficient studies as it depicts in figure 4.2. It shows that the reflection coefficient for $1mm$ center to center feeder line space (D) has the best results.
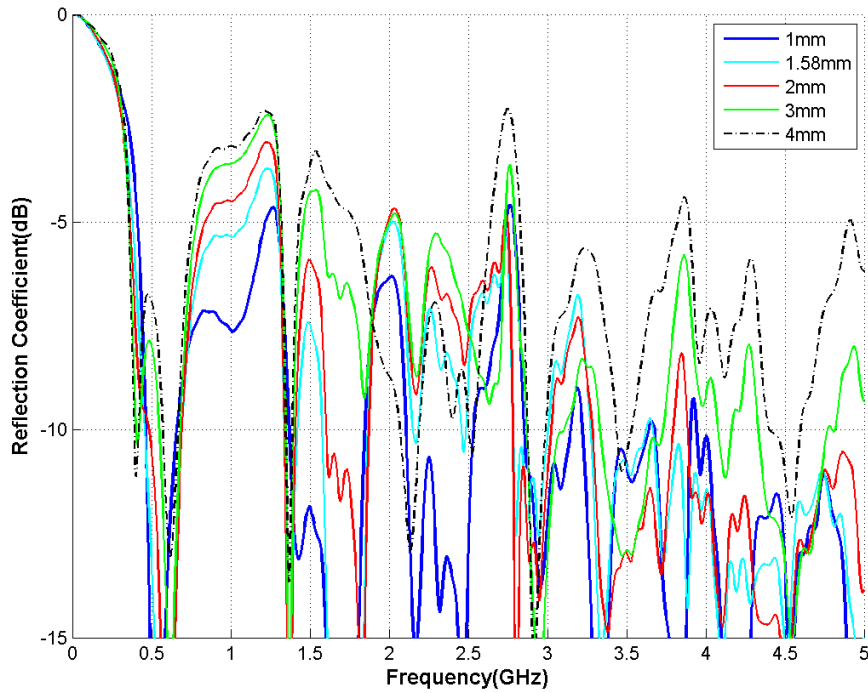

Figure 4.2: Reflection coefficient with different center to center feeder lines distance(D) in design of twin-line feeding

    The port-1 and port-2 impedances for $1mm$ feeder line distance depicts in figure 4.3 for $1mm$ distance. The impedance of port-1 is 51.62 and is almost the same as the desired value 50Ω while the simulation results for impedance of port-2 is 57.87 which is far from the desired value 20Ω which achieves by the twin-line feeding impedance of the antenna in section 3.2.3.

    The impedance can reduce by increasing the width of the line, reducing the thickness of the substrate to reduce D and use high permittivity dielectric material. The first optimization stage starts by changing the substrate material or changing feeder board top width (in twin-line feeding) to $1mm$ distance as it is shown in table 4.1.

    The results in table 4.1 shows that by changing the substrate material to TMM3 with less permittivity than FR-4 and TMM10 with higher permittivity than FR-4 with two different sheet thickness(h), the port-2 impedance will be changed but it will be far from the desired value. If the thickness of TMM3 and TMM10 increases, the port-2 impedance decreases but it is not much. By increasing the top width of the feeder board to $1mm$ and $2mm$, the port-2 impedance starts to decrease but it does not reach to desire value either. Since the port-1 impedance calculates from equation 3.2 to 3.7 for connecting to coaxial cable, it is always near desired value. It seems by changing the feeder board top width (in twin-line feeding), the impedance can decrease. Since the feeder line distance is $1mm$ and they are very close together, it is impossible to increase the width from two side because of electrical connection between feeder and ground board. Therefore, the width only increases from one side as it shows in figure 4.4.

    Since the manufacture of the antenna with $1mm$ feeder line distance is very difficult and the
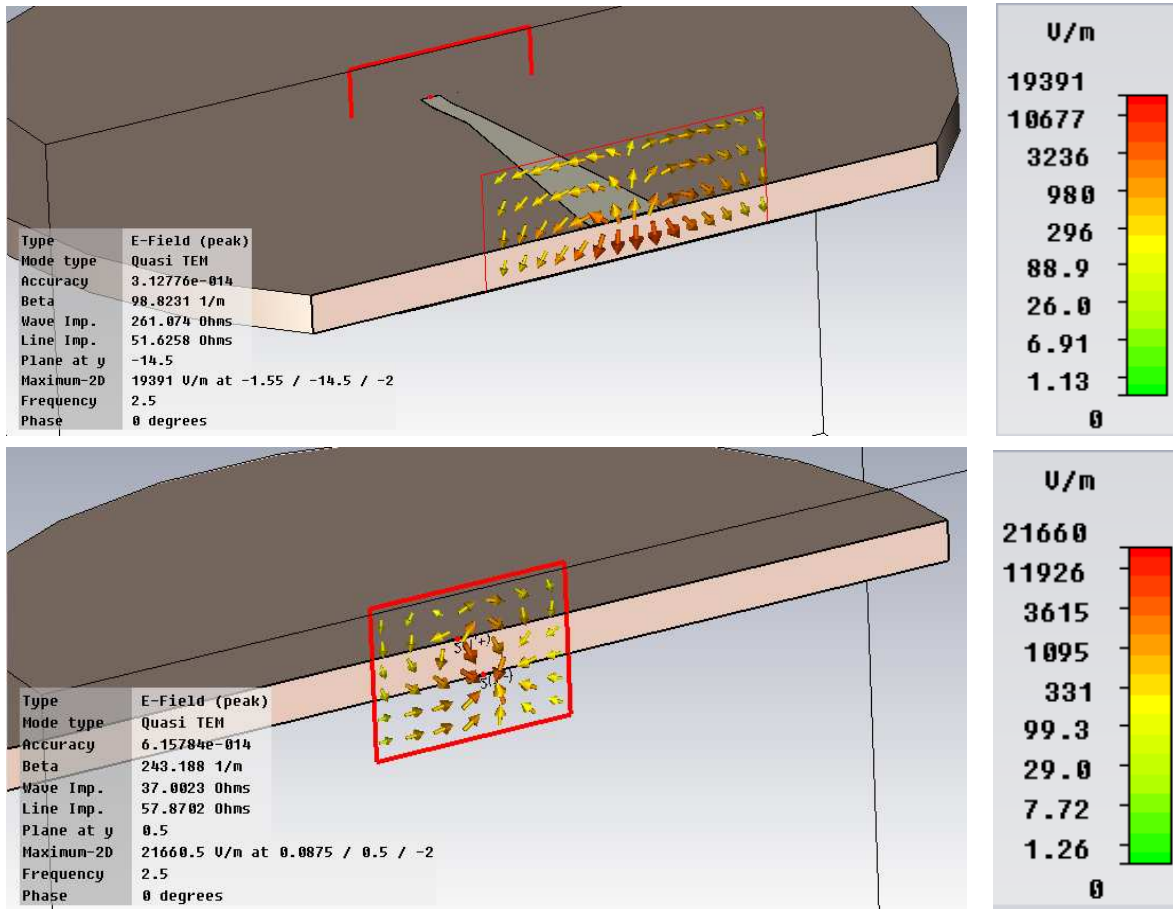
Figure 4.3: Ports impedance for 1*mm* feeder line distance with FR-4 board; The port-1 to the top and port-2 to the bottom

Table 4.1: parameter study of Ports impedance for 1*mm* feeder line distance (D) by changing the substrate material and top width of feeder board

Substrate Material	Permittivity- ϵ_r (F/m)	Top Width (*mm*)	Thickness (h)	Track Width (*mm*)	Port-1 Impedance	Port-2 Impedance
FR-4	4.3	0.825	1.6	3.1	51.62	57.87
FR-4	4.3	1	1.6	3.1	51.66	53.20
FR-4	4.3	2	1.6	3.1	51.63	44.27
TMM3	3.27	0.825	0.762	1.8	51.65	71.73
TMM3	3.27	0.825	1.27	3	51.99	63.82
TMM10	9.2	0.825	0.762	0.8	53.08	63.32
TMM10	9.2	0.825	1.27	1.3	46.25	49.08
Desired Values					50	20

feeder board top width can increase only from one direction, the feeder line distance increase to 4 and 3*mm*. The results in table 4.2 show the increasing of port-2 impedance.

It shows that the port-2 impedance of 3*mm* feeder line distance have less difference with desired value compare to 4*mm* distance as in table 4.2. The feeder board top width increases as table 4.3 to improve the impedance and be closer to desired value.
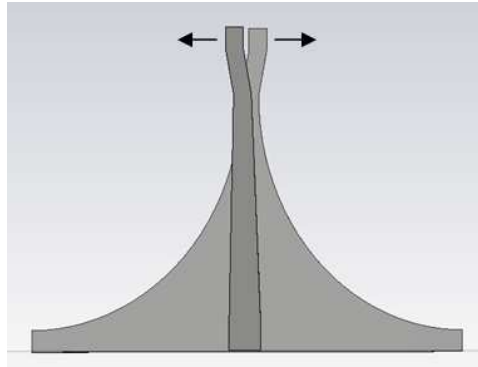
Figure 4.4: Increasion of feeder board top width from only one direction

Table 4.2: Change the feeder line distance with FR-4 board and compare port-2 impedance with desired value

FeederLine Distance(*mm*)	Top Width (*mm*)	Thickness (h)	Track Width (*mm*)	Port-1 Impedance	Port-2 Impedance	Desired Values
1	0.825	1.6	3.1	51.62	57.87	20
3	0.825	1.6	3.1	51.64	84.48	42.60
4	0.825	1.6	3.1	51.58	101.26	50

Table 4.3: The ports impedance of 3*mm* feeder line distance with FR-4 board for different feeder board top width

Top Width (*mm*)	Thickness (h)	Track Width (*mm*)	Port-1 Impedance	Port-2 Impedance
0.825	1.6	3.1	51.64	84.50
1	1.6	3.1	51.59	78.79
1.5	1.6	3.1	51.64	67.82
1.75	1.6	3.1	51.60	61.78
2	1.6	3.1	51.64	56.66
2.5	1.6	3.1	51.61	49.01
	Desired Values		50	42.60

The result in table 4.3 shows that by increasing the feeder board top width, the port-2 impedance is decreasing. The feeder board 2.5*mm* top width has the best port-2 impedance and it is near the desired value for 3*mm* feeder line distance.

The reflection coefficient for different feeder board distance depicts in figure 4.5 and emphasize more that the 2.5*mm* feeder board width is the best selection for design.

4.1.3 Two Antennas in front of each other

The reflection coefficient of two antenna in front of each other related to section 3.2.4 in dB scale and the results of equation 3.8 are depicted in figure 4.6. The results show that for higher frequencies term 3.8 is smaller than -3dB, so there is some leakage and some radiation goes out. However, for lower frequencies there is not any leakage.

The E-field and H-field pattern in x and y planes at 5 GHz frequency are depicted in figures 4.7 and 4.8. They show most of the power is absorbed. Therefore, small part of power is
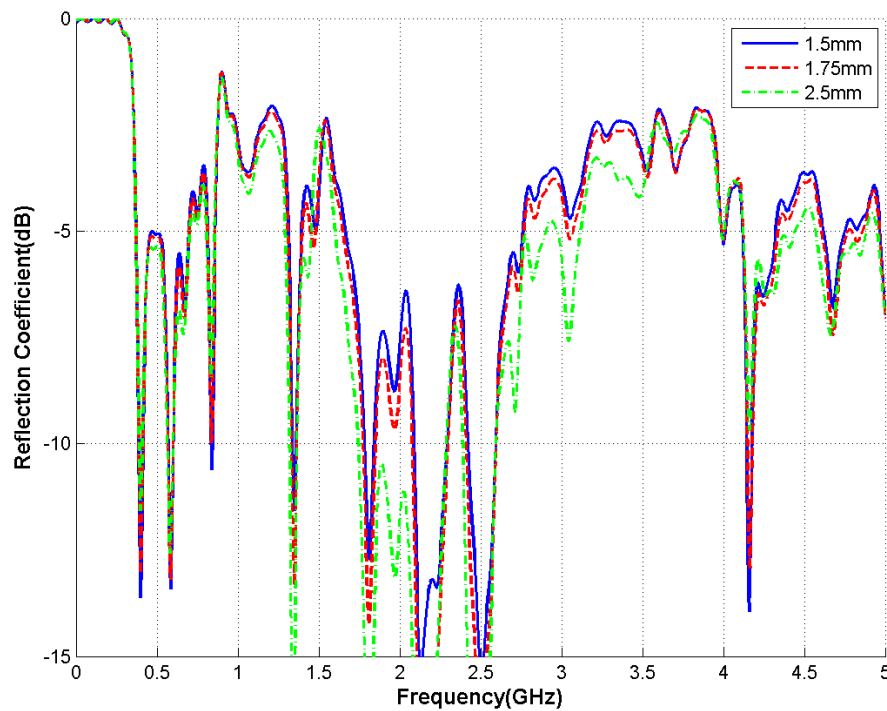
Figure 4.5: Reflection coefficient for different feeder board top width of $3mm$ feeder line distance including simple head model

radiated out of the skull.

This method for showing the antenna is directional is not very accurate, because parts of the power is refracted back from the second antenna and this causes the leakage in higher frequencies.
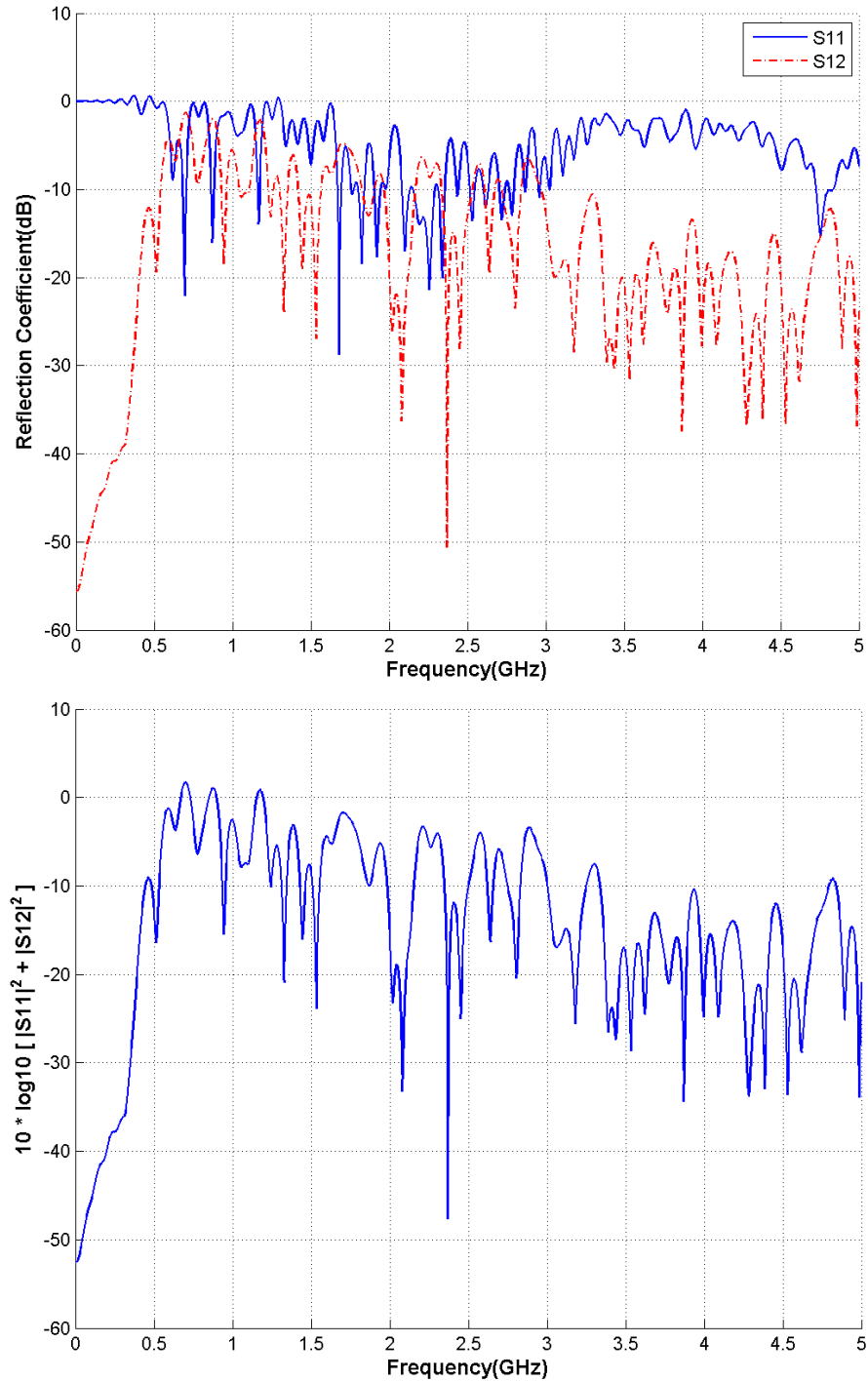
Figure 4.6: The two antennas reflection coefficient in dB, to the top and the results of power absorbed by the head to the bottom
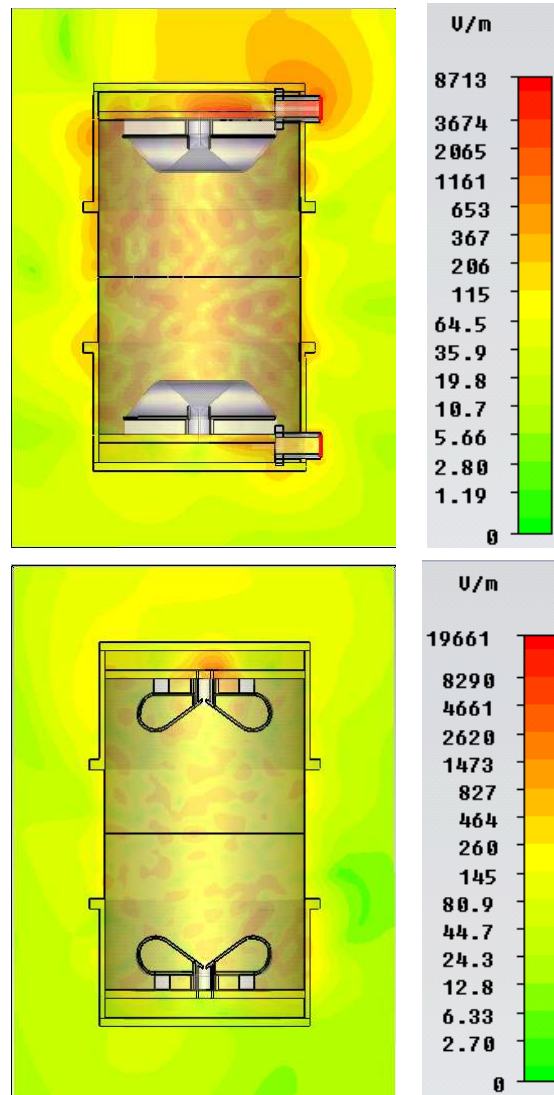
Figure 4.7: The E-field radiation pattern in x-plane, to the top and in y-plane to the bottom
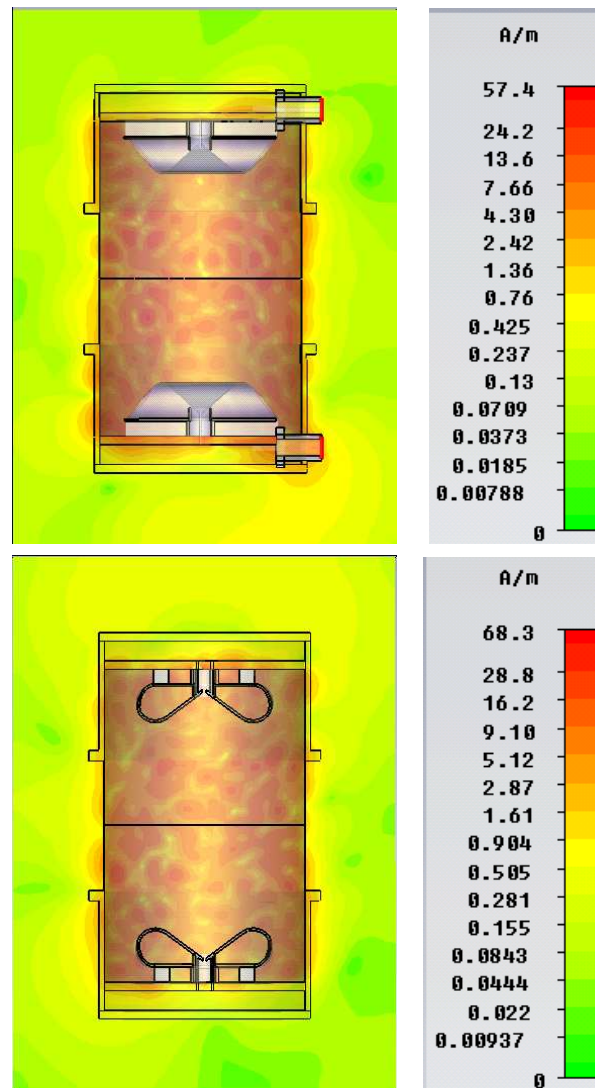
Figure 4.8: The H-field radiation pattern in x-plane, to the top and in y-plane to the bottom

4.1.4 Simulated field distribution inside the head

Figure 4.9 shows the simulated H-field distribution inside the simple model of the head. It can be observed that the wave is mainly propagated into the head, little is propagated into free space, and the field attenuation inside the head is quite big due to the big loss of the brain tissue. More study on SAR value distribution is considered in 4.1.5.

(a) 0.5 GHz   (b) 1 GHz

(c) 2 GHz   (d) 3 GHz

Figure 4.9: The simulated H-field distribution inside the head.

4.1.5 Specific energy Absorption Rate (SAR)
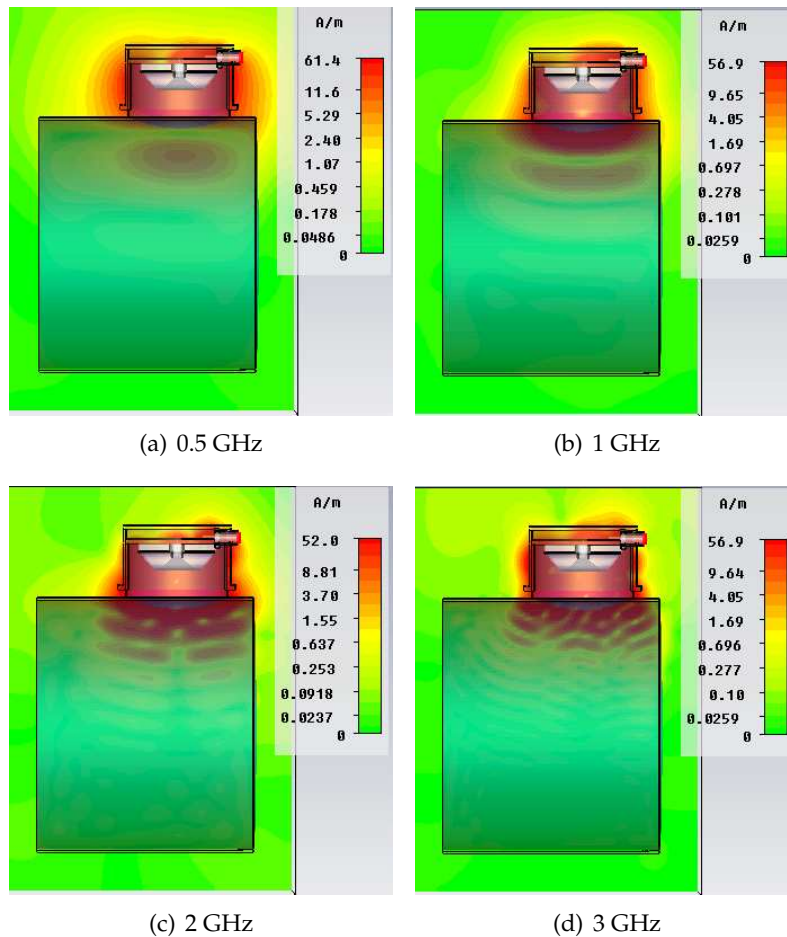
The calculations have done by CST MWS for 10g mass. The SAR distribution in the simple head model for 4 GHz frequency is shown in figure 4.10. The maximum SAR value for this frequency is 8.93, the place of maximum SAR points in different frequencies are depicted in figure 4.11. It shows that the maximum SAR points are almost in the same area of head for different frequencies.
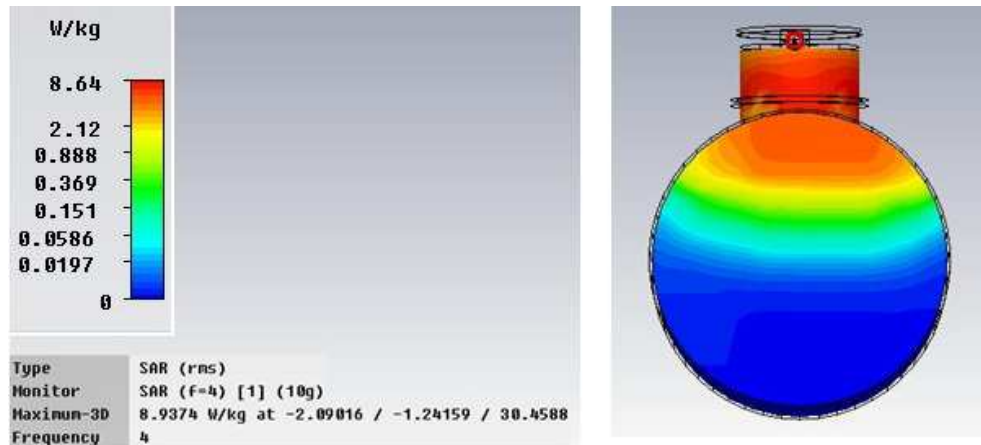

Figure 4.10: SAR distribution in 4 GHz frequency for simple head model; the maximum value of SAR and it's Cartesian coordinate are shown in the left bar
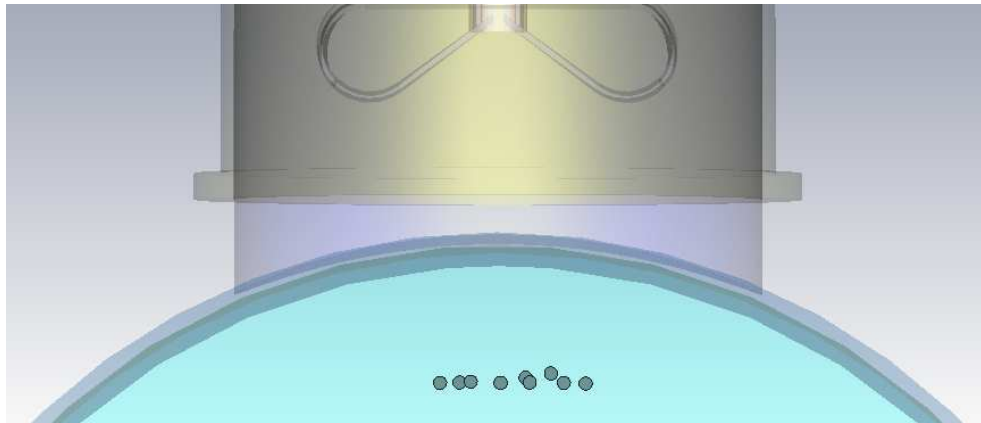
Figure 4.11: The maximum points for SAR values of different frequencies in table 4.4; from left to right points corresponds to 0.2, 1.5, 2, 0.5, 4, 3.5, 3, 1 and 2.5 GHz

The results of maximum SAR for selected frequencies and their corresponding ICNIRP basic restrictions are shown in table 4.4. As it is described in section 2.6 for multifrequency SAR should calculate by using equation 2.6 and be averaged over 6min period. For instance, by using calculated localized SAR for four frequencies (0.5, 1, 1.5 and 2 GHz) and by averaging over 6 minutes, the possible exposure time calculates according to equation 4.1 to follow ICNIRP basic restrictions of occupational.

Table 4.4: The calculated SAR for different frequencies average over 10g mass

| Frequency (GHz)	Calculated Localaized SAR (W/Kg)	Basic Restriction of Localized SAR (head and trunk) (W/Kg)
0.2	0.016	10
0.5	14.7	10
1	12.15	10
1.5	7.83	10
2	19	10
2.5	21.14	10
3	14.11	10
3.5	9.05	10
4	8.93	10

$$\frac{(14.7 + 12.15 + 7.83 + 19)}{10} \times \frac{ExposureTime}{360} \leq 1 \tag{4.1}$$

Then

$$ExposureTime = 66 Seconds$$

The calculated exposure time for previous example shows that in average we should have 5 minutes rest in each 6 minutes to follow the ICNIRP guideline. The proposed pulse train for exposure and rest time is depicted in figure 4.12.
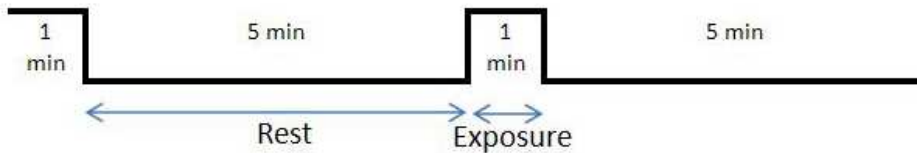
Figure 4.12: The sample of possible exposure pulse for four frequencies

The ICNIRP guideline provided restrictions for general public and occupational. However, the designed antenna is directional and exposure outside the body of detection is negligible. Therefore, only the patient should be considered. The ICNIRP guideline does not provide any restrictions for diagnosis purpose. Anyway, we considered the restrictions as occupational. The described calculations is for one antenna on the head. However, diagnosis system consists of antenna array and it should be studied further.

4.2 Final Design

The antenna after doing an optimal design procedure considers as final version and simulated with simple and real phantom as describes in section 3.2.2. The reflection coefficient with shell and without shell depicts in figure 4.13. It is obvious, that the whole system is ultra-wide multi-band (UWMB) instead of UWB and the results of with shell and without shell are almost the same.
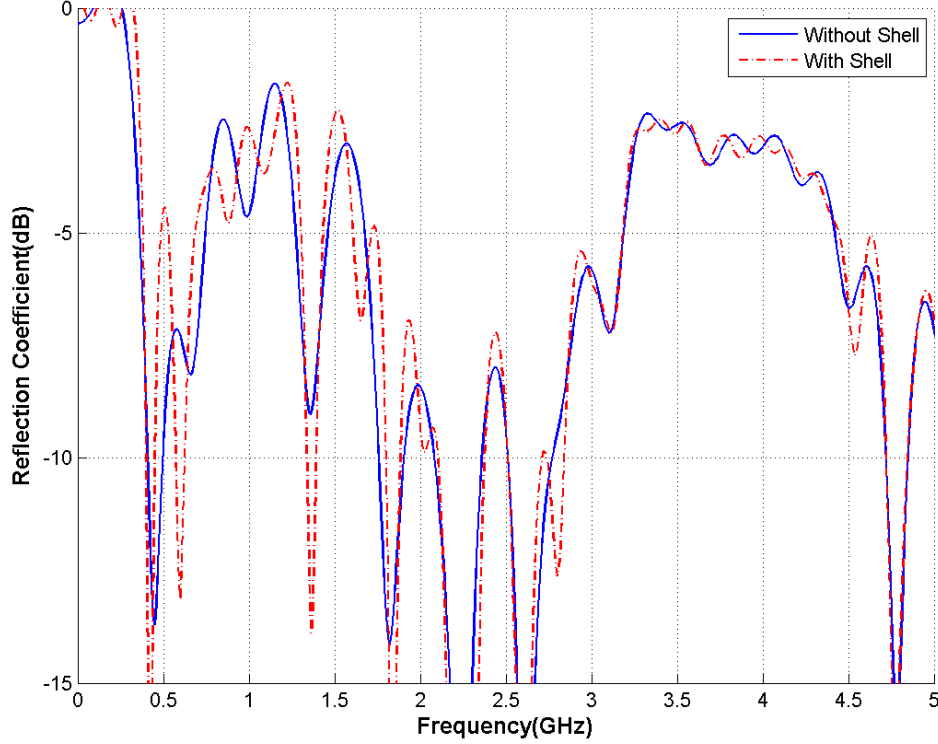

Figure 4.13: Reflection coefficient of the final design; with shell and without shell

The total radiation efficiency as a function of frequency for final design is depicted in figure 4.14. It shows almost all the power is absorbed through the skull and the amount of losses are negligible. This is indicated that the antenna is directional.

The amplitude of the reflection coefficient in dB is calculated by equation 4.2.

$$|A/A_{ref}|_{dB} = 20.log|A/A_{ref}|dB \qquad (4.2)$$

alternatively, it is calculated by equation 4.3.

$$|P/P_{ref}|_{dB} = 10.log|P/P_{ref}|dB \qquad (4.3)$$

where P is the power density.

The amount of $A = 10^{\frac{A_{dB}}{20}}$ indicates the amount of leakage and the amount of 1 - A indicates the amount of absorbed value. The more the amount of A decreases, the more power is absorbed by head as shows in figure 4.14.
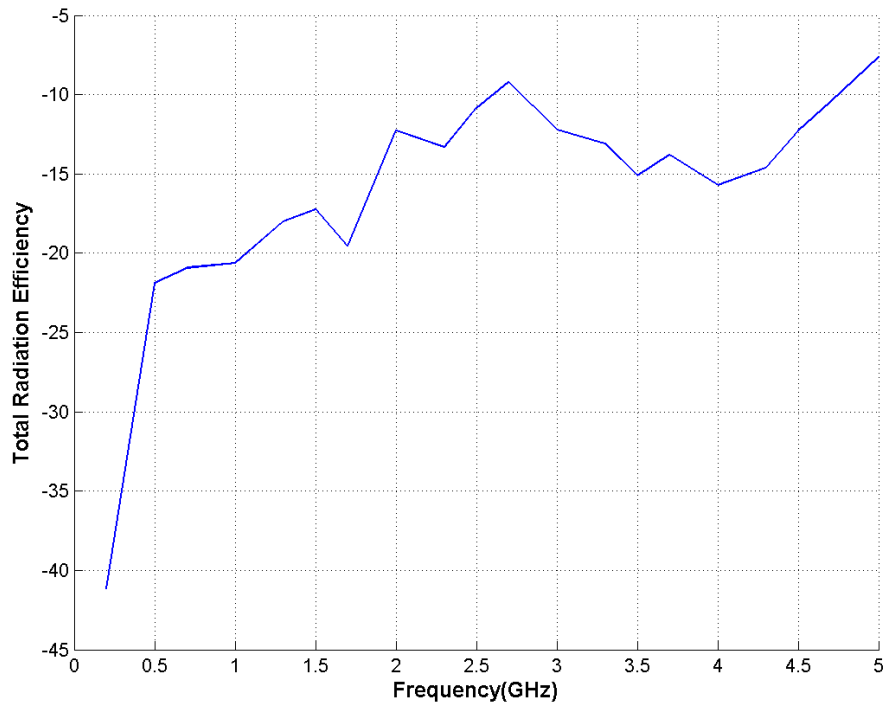
Figure 4.14: The total radiation efficiency

4.2.1   Real Phantom Simulation

The real phantom reflection coefficient for final design simulation related to figure 3.11 depicts in figure 4.15. This also indicates it has UWMB performance.
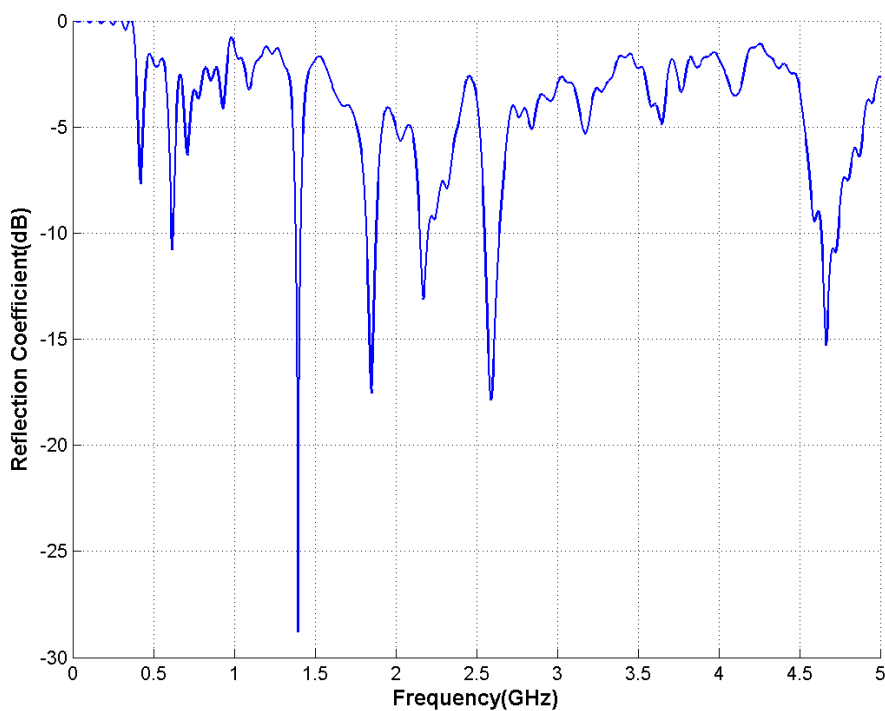

Figure 4.15: The final design S-parameter for real phantom as human head model

4.3 Measurements

In this part the measurement results are discussed.

4.3.1 Antenna Measurement

Two prototype of the antennas has been manufactured which has a size of $28 \times 28 \times 11mm^3$ and the water cylinder is $25mm$ height with a diameter of $46mm$ as it is depicted in figure 4.16. The measurements had done and results are illustrated in this section.
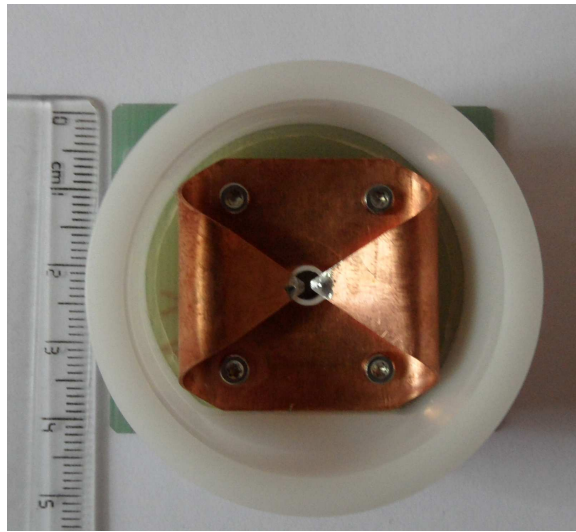
Figure 4.16: The manufactured antennas

Reflection coefficient of antenna alone

The reflection coefficient of two antennas without water and with water are measured by Aglient E5071C network analyzer and the results are shown in figure 4.17.

As it is obvious, two antennas have almost the same S-parameter results. The antennas without water work above 4 GHz frequency range. It is not unexpected because the impedance matching is designed based on with water. The S-parameter results for antennas in water have multi band frequencies in frequency range between 1 to 2 GHz and in this range it has less reflection from antenna.
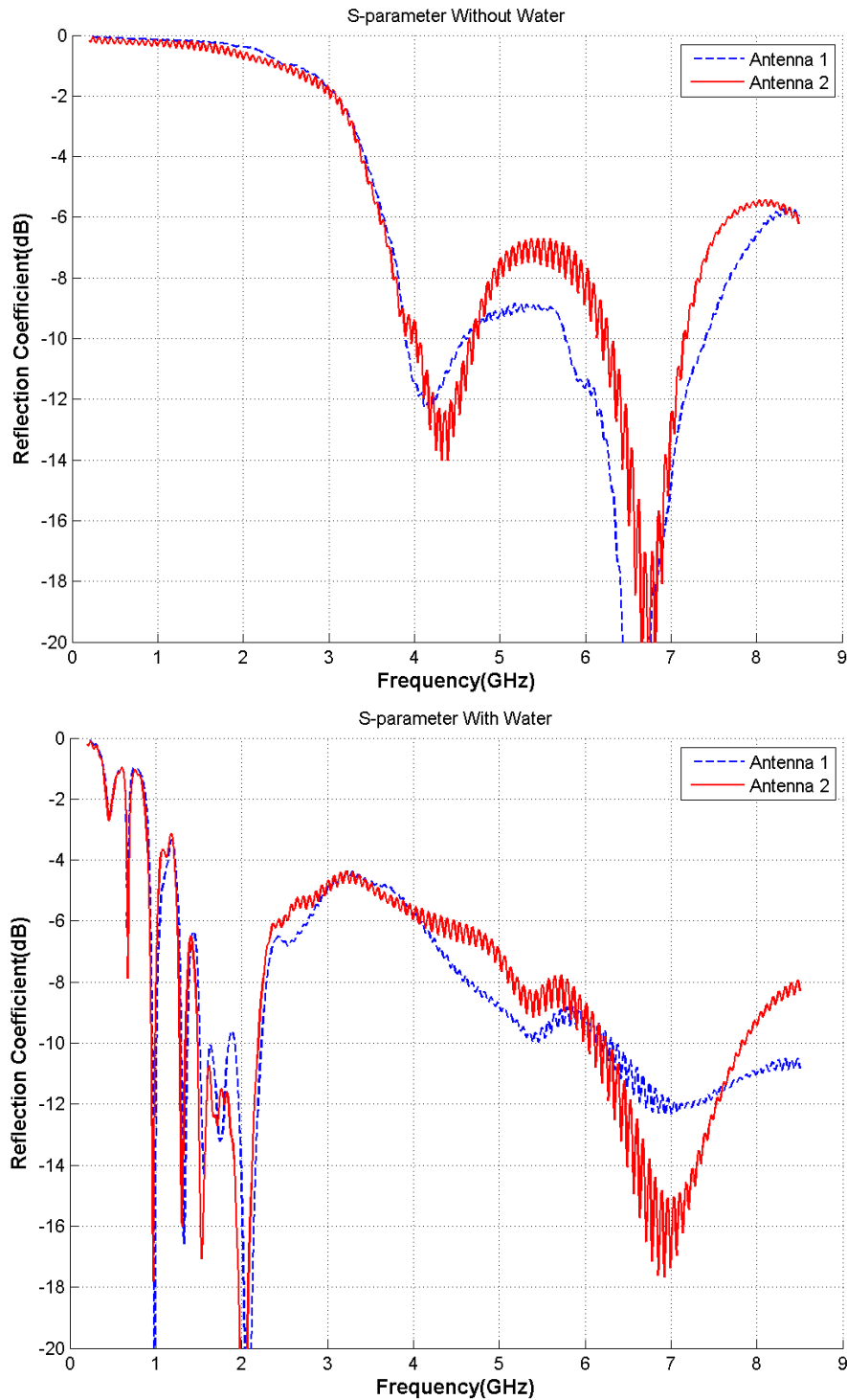
Figure 4.17: Reflection coefficient for two manufactured antennas;without and with water to top and bottom, respectively

Antenna alone in RC

The total radiation efficiency and the reflection coefficient are calculated by placing the antenna in the RC. The radiation leakage-out ratio is calculated by equation 4.4.

$$e_{rad} = e_{totrad}(dB) - 10log_{10}(1 - |S11|^2) \tag{4.4}$$

Where $S11$ = Reflection Coefficients

    The results are depicted in figure 4.18 and 4.19. It can be observed that, the peak value of the radiation leakage-out ratio is below -10 dB, which is a very good performance for this work.
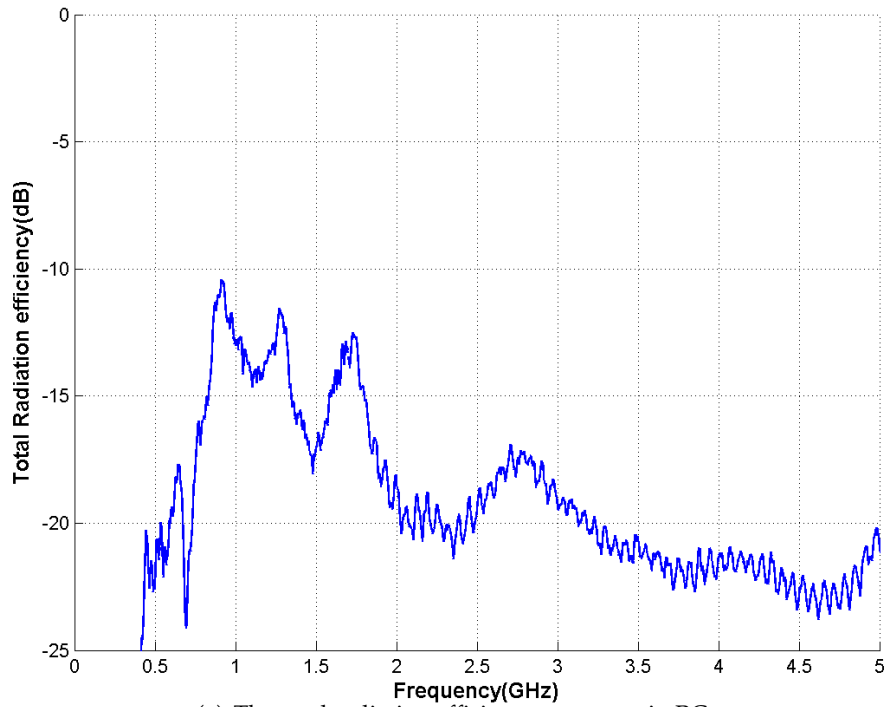
(a) The total radiation efficiency measures in RC
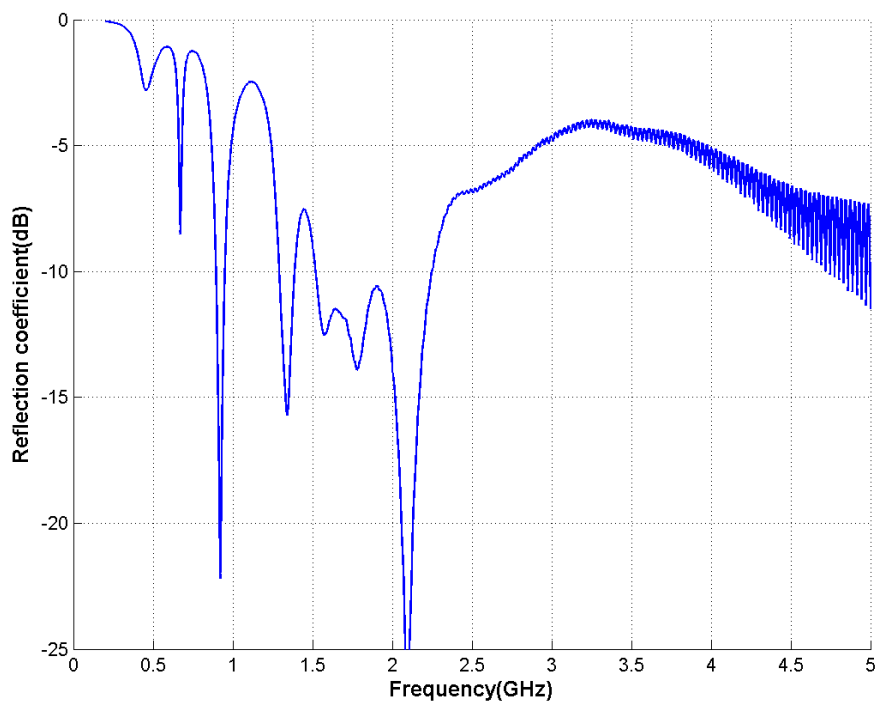
(b) The reflection coefficient measures in RC

Figure 4.18: The antenna measurements with tap water in RC; the total radiation efficiency in (a) and the reflection coefficient in (b)
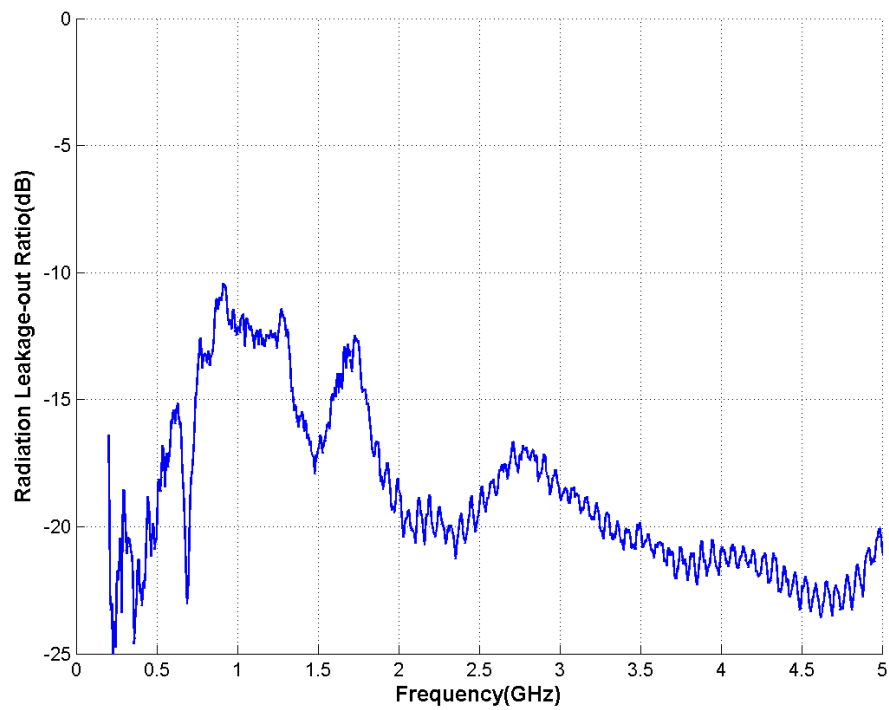
Figure 4.19: Measurement of radiation leakage-out ratio in RC calculated by equation 4.4

Two antennas in front of each other

Two antennas with water as showing in figure 4.20 are placed in front of each other. Also, the reflection coefficient are depicted in figure 4.23. It shows that the transmission coefficient between two antennas (S12) is small i.e, small part of power from one antenna is reached to the other antenna. This could be because of lossy tap water.
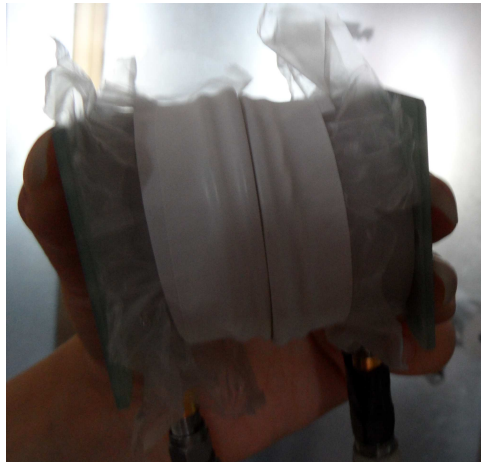
Figure 4.20: Two antennas in front of each other to study reflection coefficient
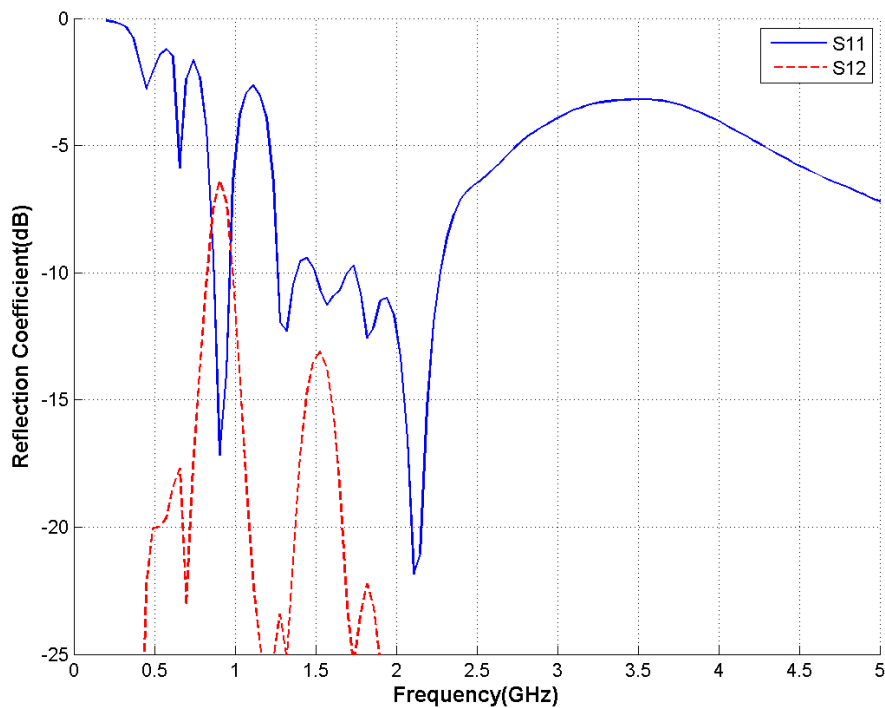
Figure 4.21: Reflection coefficient of the two antennas in front of each other

4.3.2 Real Phantom Measurements

Antenna on phantom head measurement

The antenna on the phantom head and the reflection coefficient are depicted in figures 4.22 and 4.23. It is obvious that the reflection coefficient is UMWB.

Figure 4.22: The phantom head with one antenna on top to measure S-parameter
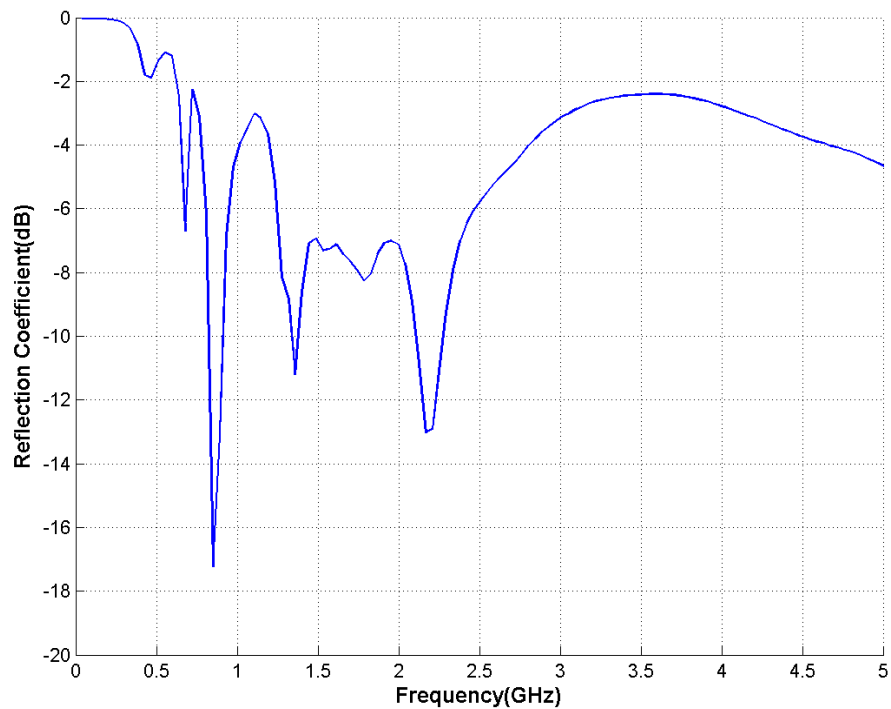
Figure 4.23: Reflection Coefficient of the antenna on the phantom head

Antenna on phantom head In the reverberation chamber

The total radiation efficiency and the reflection coefficient are calculated by placing the antenna on the phantom in the RC. The measurement results are depicted in figure 4.24 and 4.25. The peak value of the radiation leakage-out ratio is below -10 dB, which indicated a good performance. The discontinuity in the results is due to the Bluetest software error.
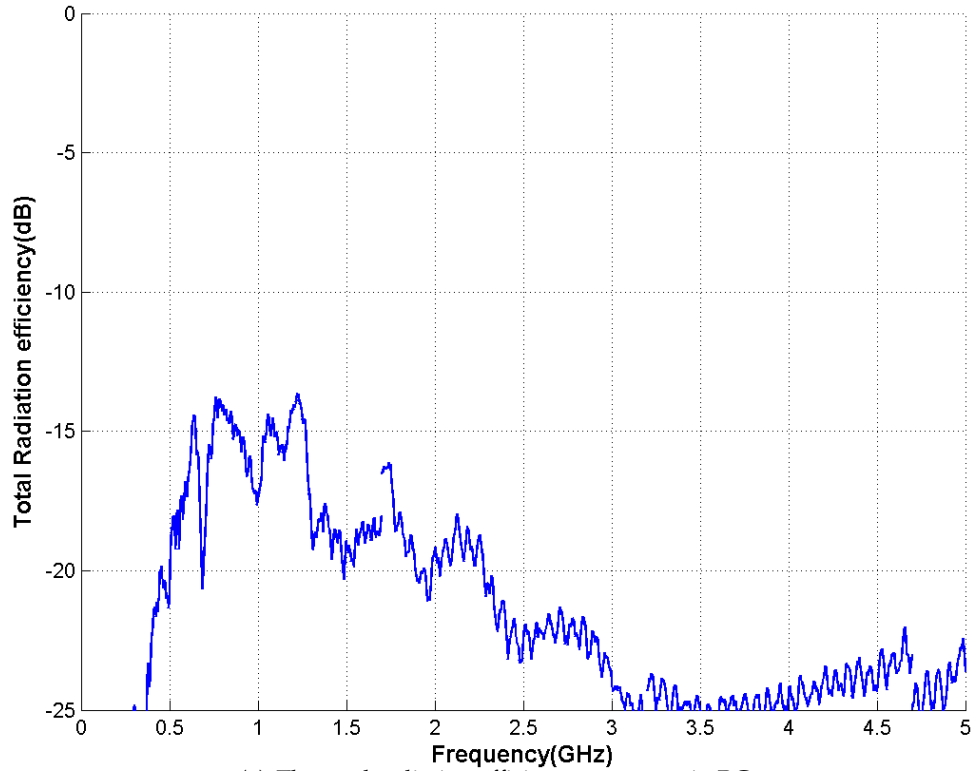
(a) The total radiation efficiency measures in RC
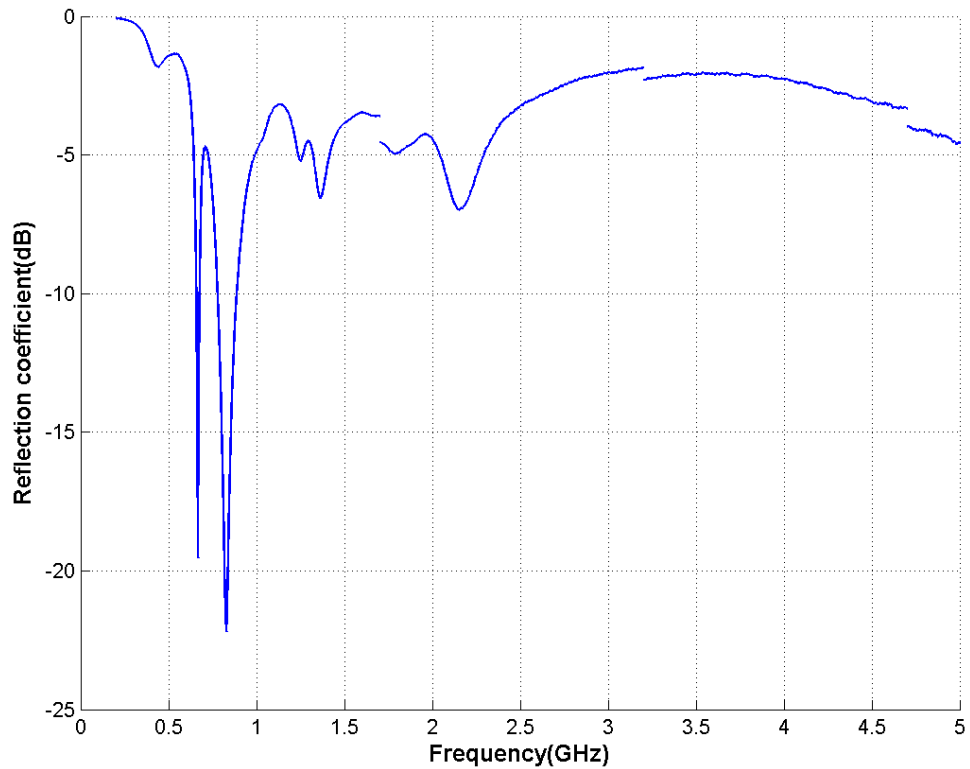
(b) The reflection coefficient measures in RC

Figure 4.24: The antenna measurements on phantom head in RC; the total radiation efficiency in (a) and the reflection coefficient in (b)
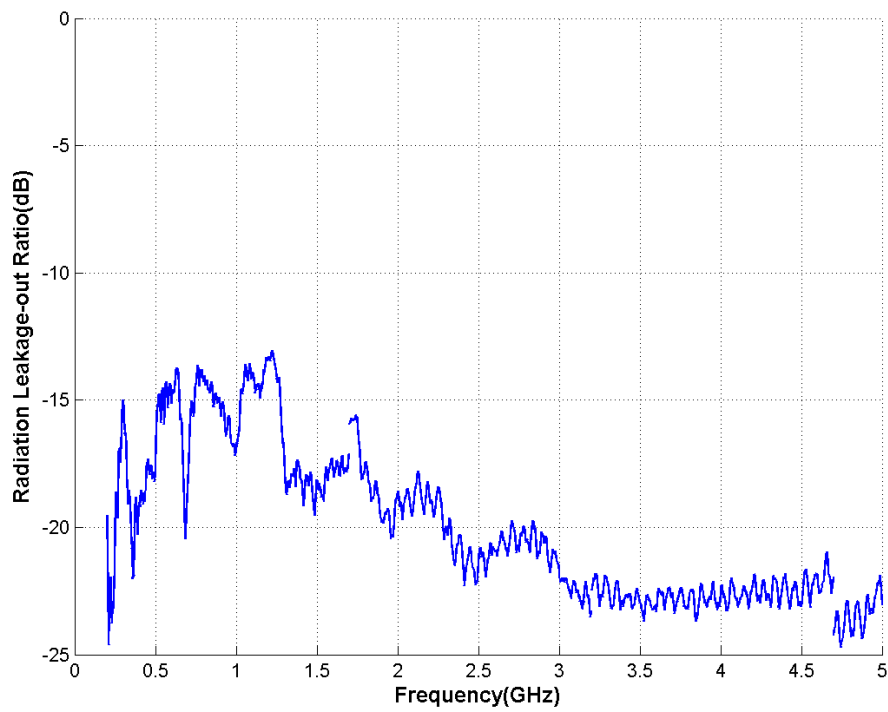
Figure 4.25: The radiation efficiency calculated by equation 4.4

4.3.3 Compare existing antenna versus self-grounded Bow-Tie

The new antenna is compact and directional compare to the existing antenna in Medfield. Also, the reflection coefficient of the new antenna shows the better performance of the new antenna model as depicts in figure 4.26.
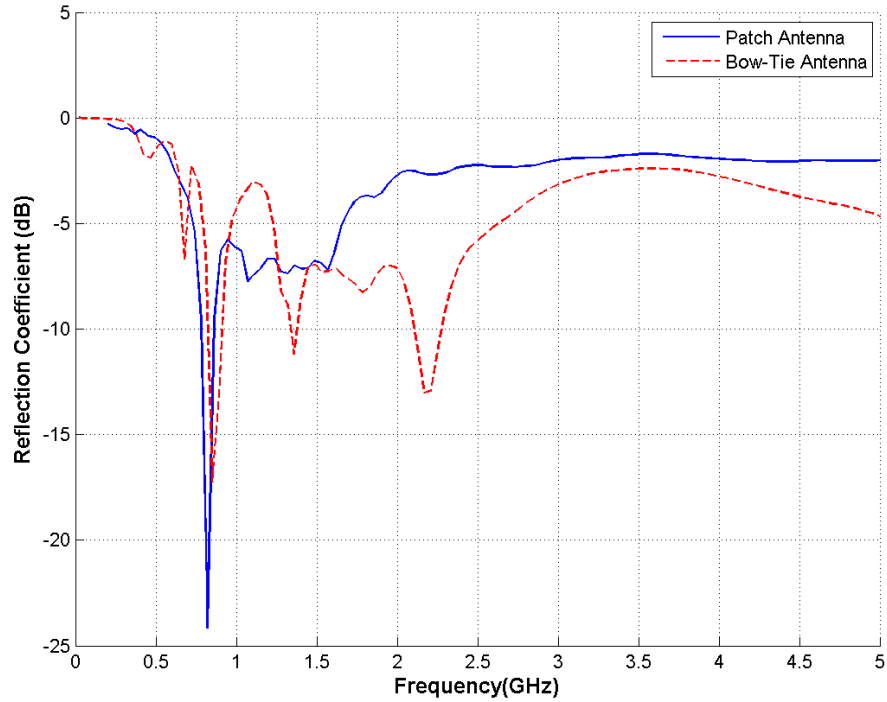
Figure 4.26: Compare reflection coefficient of the existing antenna and self-grounded Bow-Tie antenna

5

Conclusion

A compact water-filled self grounded Bow-Tie antenna for stroke diagnosis is presented. The antenna has ultra-wide multi-band (UWMB) performance over the frequency range of 0.5 - 5 GHz, with good reflection coefficient, low radiation leakage-out ratio and very compact size.

The skull with permittivity of 50 between distilled water and brain, makes a UWB performance of reflection coefficient very difficult for the whole antenna system. An ultra-wide multi-band (UWMB) performance is more realistic for the antenna system in this work.

6

Future Work

The antenna will be immersed in other liquids with different permittivity and study if the reflection coefficient is improved.

More prototype of antennas will manufacture to study the antenna array and coupling between antennas and the signal processing should be done.

Simulation and measurement of antenna can be used for other application such as microwave tomography of breast cancer.

Simulate and measurement of antenna with a mass with dielectric properties of the blood in the phantom head and study the reflection coefficient of the antenna.

Bibliography

[1] S. Semenov, "Microwave tomography: review of the progress towards clinical applications," *Philosophical Transactions of the Royal Society A: Mathematical, Physical and Engineering Sciences*, vol. 367, no. 1900, p. 3021, 2009.

[2] S. Abtahi, J. Yang, and S. Kidborg, "Compact immersed 0.5 - 3 GHz self-grounded bow-tie antenna for stroke diagnosis," *Antennas and Wireless Propagation Letters, IEEE*, submitted, September 2011.

[3] E. Widmaier, H. Raff, K. Strang, and A. Vander, *Human physiology: the mechanisms of body function*. Mcgraw Hill, 2008.

[4] WorldStrokeAcademy, "Let's talk about a stroke diagnosis," vol. 2011, no. 20 May, 2007.

[5] Y. Serguei *et al.*, "Microwave tomography for brain imaging: Feasibility assessment for stroke detection," *International Journal of Antennas and Propagation*, vol. 2008, 2008.

[6] A. Fhager, "Microwave tomography," Ph.D. dissertation, Chalmers tekniska hogskolan, 2006.

[7] J. Powell, "Antenna design for wideband radio," Ph.D. dissertation, Massachusetts Institute of Technology, 2001.

[8] C. Balanis, *Antenna theory*. Wiley New York, 1997.

[9] K. Rosengren and P. Kildal, "Radiation efficiency, correlation, diversity gain and capacity of a six-monopole antenna array for a mimo system: theory, simulation and measurement in reverberation chamber," in *Microwaves, Antennas and Propagation, IEE Proceedings-*, vol. 152, no. 1. IET, 2005, pp. 7–16.

[10] H. Trefna and M. Persson, *Antenna array design for brain monitoring*, 2008.

[11] G. Brown and O. Woodward, "Experimentally determined radiation characteristics of conical and triangular antennas," *RCA rev*, vol. 13, no. 4, pp. 425–452, 1952.

[12] O. LODGE, "Oliver joseph lodge," Aug. 16 1898, uS Patent 609,154.

[13] D. Isbell, "Log periodic dipole arrays," *Antennas and Propagation, IRE Transactions on*, vol. 8, no. 3, pp. 260–267, 1960.

[14] R. Olsson, P. Kildal, and S. Weinreb, "The Eleven antenna: a compact low-profile decade bandwidth dual polarized feed for reflector antennas," *Antennas and Propagation, IEEE Transactions on*, vol. 54, no. 2, pp. 368–375, 2006.

[15] J. Yang, M. Pantaleev, P. Kildal, B. Klein, Y. Karandikar, L. Helldner, N. Wadefalk, and C. Beaudoin, "Cryogenic 2-13 ghz eleven feed for reflector antennas in future wideband radio telescopes," *Antennas and Propagation, IEEE Transactions on*, no. 99, pp. 1–1, 2011.

[16] Y. Mushiake, "Self-complementary antennas," *Antennas and Propagation Magazine, IEEE*, vol. 34, no. 6, pp. 23–29, 1992.

[17] P. Gibson, "The vivaldi aerial," in *Microwave Conference, 1979. 9th European*. IEEE, 1979, pp. 101–105.

[18] J. Yang and A. Kishk, "The self-grounded bow-tie antenna," in *2011 IEEE International Symposium on Antennas and Propagation, Spokane, USA, 3-8 July, 2011*, 2011.

[19] P. J. Gibson, "The vivaldi aerial," *Proc. 9th European. Microwave Conference*, pp. 101–105, 1979.

[20] T. Vu, M. Dooghabadi, S. Sudalaiyandi, H. Hjortland, O. Naess, T. Lande, and S. Hamran, "Uwb vivaldi antenna for impulse radio beamforming," in *NORCHIP, 2009*. IEEE, pp. 1–5.

[21] J. Yang, "On periodicity of input impedance of log-periodic array antennas," *IEEE Transactions on Antennas and Propagation*, submitted, 2011.

[22] J. Yang, M. Pantaleev, P.-S. Kildal, and L. Helldner, "Design of compact dual-polarized cryogenic 1.2 - 10 GHz Eleven feed for decade bandwidth radio telescopes," *IEEE Transactions on Antennas and Propagation*, submitted, June 2011.

[23] J. Yang and P. Kildal, "Optimization of reflection coefficient of large log-periodic array by computing only a small part of it," *IEEE Trans. Antennas Propagat.*, vol. 59, no. 6, pp. 1790–1797, June 2011.

[24] J. Yang, D. Nyberg, and J. Yin, "Impedance matrix of a folded dipole pair under eleven configuration," *Microwaves, Antennas & Propagation, IET*, vol. 4, no. 6, pp. 697–703, 2010.

[25] J. Yang, "On conditions for constant radiation characteristics for log-periodic array antennas," *Antennas and Propagation, IEEE Transactions on*, vol. 58, no. 5, pp. 1521–1526, 2010.

[26] A. Yasin, J. Yang, and T. Ostling, "A compact dual-band feed for reflector antennas based on choke horn and circular eleven antenna," *IEEE Transactions on Antennas and Propagation*, vol. 57, no. 10, pp. 3300–3302, 2009.

[27] P. Hall, "The square kilometre array: An international engineering perspective," *The Square Kilometre Array: An Engineering Perspective*, pp. 5–16, 2005.

[28] A. Niell, A. Whitney, B. Petrachenko, W. Schl
"uter, N. Vandenberg, H. Hase, Y. Koyama, C. Ma, H. Schuh, and G. Tuccari, "VLBI2010: current and future requirements for geodetic VLBI systems," *Report of Working Group*, vol. 3, 2005.

[29] P.-S. Kildal, "The hat feed: a dual-mode rear-radiating waveguide antenna having low cross polarization," *IEEE Trans. Antennas Propagat.*, vol. 35, no. 9, pp. 1010–1016, Sept. 1987.

[30] J. Yang and P. Kildal, "Scattering by screw heads in reflecting surfaces and their effect on the sidelobes of reflector antennas," *Microwave and Optical Technology Letters*, vol. 38, no. 3, pp. 213–217, 2003.

[31] ——, "Calculation of ring-shaped phase centers of feeds for ring-focus paraboloids," *IEEE Transactions on Antennas and Propagation*, vol. 48, no. 4, pp. 524–528, 2000.

[32] ——, "Gaussian vertex plate improves reflection coefficient and far-out sidelobes in prime-focus reflector antennas," *Microwave and Optical Technology Letters*, vol. 21, no. 2, pp. 125–129, 1999.

[33] J. Yang and P.-S. Kildal, "FDTD design of a Chinese hat feed for shallow mm-wave reflector antennas." Atlanta, Georgia: Proc. 1998 IEEE AP-S International Symposium, 21-26 June 1998, pp. 2046–2049.

[34] W. Wei, J. Yang, T. Ostling, and T. Schafer, "New hat feed for reflector antennas realised without dielectrics for reducing manufacturing cost and improving reflection coefficient," *Microwaves, Antennas & Propagation, IET*, vol. 5, no. 7, pp. 837–843, 2011.

[35] M. Denstedt, T. Ostling, J. Yang, and P.-S. Kildal, "Tripling bandwidth of hat feed by genetic algorithm optimization." Hawai: 2007 IEEE AP-S International Symposium, 10-15 June 2007.

[36] E. Geterud, J. Yang, and T. Ostling, "Wide band hat-fed reflector antenna for satellite communications," in *Antennas and Propagation (EUCAP), Proceedings of the 5th European Conference on*. IEEE, pp. 754–757.

[37] J. Yang and A. Kishk, "A novel low-profile compact directional ultra-wideband antenna: the self-grounded Bow-Tie antenna," *IEEE Trans. Antennas Propagat.*, vol. 59, no. x, x accepted, 2011.

[38] Y. Yu, S. Maalik, J. Yang, T. McKelvey, K. Malmstrom, L. Landen, and B. Stoew, "A new uwb radar system using uwb cmos chip," in *Proceedings of the 5th European Conference on Antennas and Propagation (EUCAP)*. IEEE, pp. 771–775.

[39] Y. Yu, J. Yang, T. McKelvey, and B. Stoew, "Development of a compact UWB radar system using the self-grounded bow-tie antennas and UWB cmos chip," *IEEE Transactions on Antennas and Propagation*, submitted, May 2011.

[40] ICNIRP., "Guidelines for limiting exposure to time-varying electric, magnetic, and electromagnetic fields," *Health Physics*, vol. 74, pp. 494–522, 1998.

[41] CST Microwave Studio; http://www.cst.com.

[42] S. Gabriel, R. Lau, and C. Gabriel, "The dielectric properties of biological tissues: III. parametric models for the dielectric spectrum of tissues," *Physics in medicine and biology*, vol. 41, p. 2271, 1996.

[43] G. Schmid, G. Neubauer, and P. Mazal, "Dielectric properties of human brain tissue measured less than 10 h postmortem at frequencies from 800 to 2450 mhz," *Bioelectromagnetics*, vol. 24, no. 6, pp. 423–430, 2003.

[44] I. Bahl and R. Garg, "Simple and accurate formulas for a microstrip with finite strip thickness," *Proceedings of the IEEE*, vol. 65, no. 11, pp. 1611–1612, 1977.